

BattOpt: Optimal Facility Planning for Electric Vehicle Battery Recycling

Matthew Brun*

Xu Andy Sun†

Abstract

The electric vehicle (EV) battery supply chain will face challenges in sourcing scarce and expensive minerals required for manufacturing and in disposing of hazardous retired batteries. Integrating recycling technology into the supply chain has the potential to alleviate these issues; however, players in the battery market must design investment plans for recycling facilities. In this paper, we propose a multistage stochastic optimization model for computing minimum cost recycling capacity decisions, in which retired batteries are recycled and recovered materials are used to manufacture new batteries. To construct a realistic and high-fidelity model, we transform EverBatt, a leading evaluation framework for battery recycling cost and environmental impact, into a prescriptive decision-making tool for determining optimal investment strategies. Our model is a separable concave minimization subject to linear constraints, a class for which we design a new finitely convergent global optimization algorithm based on piecewise linear approximation that solves up to 14x faster than comparable algorithms. We propose an equivalent reformulation of the model that reduces the total number of variables by introducing integrality constraints. The reformulation can also be solved by our global algorithm with drastically reduced solve times. We detail a cut grouping strategy for a Benders’ decomposition at the operational scale which improves convergence relative to single-cut and multi-cut implementations. To produce a set of operational scenarios, we design an approach for generating time-series projections for new battery demand, retired battery supply, and material costs, leveraging state-of-the-art econometric models for critical metal prices and EV demand. We apply our model to compute optimal investment plans and quantify the impact of optimal decision-making on the supply chain. We analyze the impact of policy instruments to reveal key insights for policy makers: while recycling capacity grants and production credits both effectively encourage domestic investment in recycling, production credits are more cost effective under smaller policy budgets, whereas grants become the more cost-effective instrument as total policy expenditure increases. Finally, the optimal solutions show that effective investment in recycling can reduce battery manufacturing costs by 22% and reduce environmental impacts by up to 7%.

Key words: electric vehicle battery recycling, facility planning, global optimization, stochastic optimization

1 Introduction

Electric vehicles (EVs) are a principal technology in the energy transition that will play an important role in reducing emissions. The demand for the lithium-ion batteries that power EVs is expected to grow by over 20% year-over-year through 2030, reaching a market valuation in excess of \$360 billion (Campagnol et al. 2022). Manufacture of these batteries requires “critical minerals”, materials defined by a vulnerability to supply chain disruption, including lithium (Li), cobalt (Co), nickel (Ni), and manganese (Mn) (U.S. Geological Survey 2022). As demand for batteries grows significantly, so will the demand for these materials; for instance, lithium requirements are expected to grow 6-fold by 2030 under current climate pledges (IEA 2022).

*Operations Research Center, Massachusetts Institute of Technology, Cambridge, MA 02139. Email: brunm@mit.edu

†Sloan School of Management, Massachusetts Institute of Technology, Cambridge, MA 02139. Email: sunx@mit.edu

EV batteries have variable lifespans, but generally are retired after a capacity reduction of 20% with an expected age of 10 years (Marano et al. 2009). As large numbers of batteries are removed from vehicles, attention must be paid to their safe disposal. EV batteries contain toxic and heavy metals, so improper disposal may pose health and environmental risks (Kang et al. 2013). Further, recent European Union regulation sets recycled material composition requirements for new batteries and material recovery targets from retired batteries (Council of the European Union 2023).

In light of these challenges, a promising solution is the recycling of retired batteries, allowing for the recovery of component materials for reuse. Lithium-ion battery packs are made up of many individual cells, each of which contain a graphite-based anode, lithium-based cathode, electrolytes, binding polymers, and copper and aluminum foils, inside a plastic or steel shell. Common cathode compounds include lithium iron phosphate (LFP), lithium nickel cobalt aluminum oxide (NCA), and lithium nickel manganese cobalt oxide (NMC). Many battery materials can be recovered via recycling, although the most valuable are the metals contained in cathode compounds.

Current technologies for lithium-ion battery recycling include pyrometallurgical, hydrometallurgical, and mechanical processes (Harper et al. 2019). *Pyrometallurgical recycling* exposes battery packs to high temperatures, incinerating extraneous battery components and inducing chemical reactions to recover compounds from the cathode material (Makuza et al. 2021). *Hydrometallurgical recycling* reacts cathode materials with a leaching solution, from which compounds are precipitated (Yao et al. 2018). A newer process, referred to as *direct recycling*, uses mechanical processes such as shredding and crushing to separate and recover constituent materials, followed by “relithiation” of cathode material to restore the chemical properties of a new material (Wu et al. 2023).

EverBatt (Dai et al. 2019) is a recently proposed closed-loop model for analyzing the cost and environmental impacts of battery recycling and manufacturing with detailed, high-fidelity data for recycling process yields, facility costs, and emissions calculations. In a *closed-loop* model, recycled materials are used for the manufacturing of new products. This differs from *open-loop* models, in which recovered materials are sold or disposed. In the EverBatt model, retired batteries are first recycled. If pyrometallurgical or hydrometallurgical recycling is used, the extracted cathode precursors are remanufactured into cathode material in a step called *cathode production*. Under direct recycling, as cathode material is recovered in its original form, this step is not necessary. Then, new batteries are manufactured using the recycled cathode material and other purchased materials. Given fixed facility capacities that handle specific retired battery input and new battery output quantities, EverBatt computes the cost and environmental impact of recycling, cathode production, and manufacturing facilities across this closed-loop supply chain.

As players in the battery industry look towards incorporation of recycling technologies (Ohnsman 2022, BASF 2023), important questions surrounding investment and capacity planning will arise. Firms will decide how much recycling capacity to construct, which technologies to invest in, and when to use recycled materials to produce new batteries. In this paper, we address these questions by converting the EverBatt framework into an optimization model. We summarize our contributions in modeling, algorithmic design and computation, and analysis as follows:

1. Modeling:

- We propose a multistage stochastic optimization model for the design and operation of a closed-loop EV battery recycling supply chain. At the strategic scale, a multi-year capacity decision is made for recycling and cathode production facilities. Then, at the operational scale, decisions are made over a number of multistage scenarios on how many batteries to recycle and how to use recycled materials to manufacture new batteries. This model is a prescriptive decision-making tool built on the detailed, high-fidelity evaluation framework of battery supply chain cost and environmental impact proposed in the EverBatt tool.

- We design a methodology that leverages state-of-the-art econometric models for EV vehicle stock and critical mineral price projections to build a variety of operational scenarios for retired battery supply, new battery demand, and material cost.

2. Algorithmic design and computation:

- We propose a novel adaptive piecewise linear approximation algorithm (aPWL) for mixed-integer linearly constrained separable concave minimization that converges finitely to a globally optimal solution. In computational tests, we show that the aPWL algorithm compares favorably to benchmark algorithms, solving up to 14x faster on some instances.
- We develop an equivalent reformulation of our model that reduces the total number of variables by introducing integrality constraints. The reformulation reduces solve times from hours to minutes.
- We leverage a Benders’ decomposition approach to separate the operational scale from the strategic scale. We evaluate cut aggregation strategies within the Benders’ decomposition and show that a grouping of similar scenarios outperforms traditional single-cut and multi-cut implementations.

3. Optimal investment and policy analysis:

- We conduct extensive computational studies to analyze the impact of closed-loop recycling on new battery manufacturing. Our analysis shows that an optimal recycling investment plan in the United States reduces the expected cost of battery production by 22%, the expected energy consumption by 6%, and the expected greenhouse gas emissions by 7% through 2050, relative to a solution that does not utilize recycling. We show similar reductions on a supply chain that includes the United States and China. The optimal solutions also reveal a hidden benefit of hydrometallurgical recycling over direct recycling, as the former allows greater flexibility in the types of new batteries that can be manufactured from recycled materials.
- We analyze the impact of policy instruments, including capacity grants and production tax credits, on optimal investment and operational decisions. Our analysis reveals key insights for policy makers. We show that both recycling capacity grants and production credits encourage domestic investment in recycling capacity. However, production credits are more cost effective under smaller policy budgets, whereas grants become the more cost-effective instrument with greater total policy expenditure.

The remainder of the paper is organized as follows. In Section 2, we review relevant literature. In Section 3, we introduce our models for investment planning in the EV battery recycling supply chain. In Section 4, we propose a novel algorithm for solving linearly constrained separable concave minimization problems and a scale decomposition scheme. In Section 5, we describe our sources of data and a process for multistage scenario construction. In Section 6, we show computational results on a variety of test problems, analyze representative optimal investment decisions, and discuss the impact of policy instruments on the supply chain. In Section 7, we conclude the paper.

2 Literature Review

2.1 Battery Recycling Optimization

Capacity planning problems for manufacturing applications have been studied extensively in the literature. For thorough reviews, see Van Mieghem (2003) and Martínez-Costa et al. (2014). Many studies consider a discrete set of feasible capacity decisions. We instead focus on formulations with concave costs and continuous decisions. In this problem class, Lee and Luss (1987) and Rajagopalan et al. (1998) simplify the continuous space to a discrete set of potentially optimal decisions and solve the problem via dynamic programming. Li and Tirupati (1994)

similarly compute a finite set of candidate capacities and propose heuristic algorithms. In this work, we introduce a reformulation by identifying an underlying structure of optimal decisions, but do not enumerate all such solutions.

Previous work has explored the application of capacity and logistics planning to EV battery recycling networks. Hoyer et al. (2015), Tadaros et al. (2022), and Rosenberg et al. (2023) study open-loop battery recycling processes. Hoyer et al. (2015) propose a mixed-integer linear program (MILP) for a deterministic multi-period model that optimizes capacity decisions for battery disassembly, conditioning, and recycling facilities in Germany. Feasible capacity decisions are restricted to a discrete set of values, modeled by the construction of “modules” with fixed capacities. Tadaros et al. (2022) and Rosenberg et al. (2023) also propose multi-period deterministic MILPs for planning of open-loop EV battery recycling, the former for the Swedish supply chain and the latter the German. Tadaros et al. (2022) formulate the problem as a facility location problem with fixed capacities, while Rosenberg et al. (2023) optimize both the planned location of a facility as well as its capacity, selected from a discrete set of possible capacity levels.

Li et al. (2018), Wang et al. (2020), and Li et al. (2023) introduce models for closed-loop battery recycling. Li et al. (2018) propose a multi-period model with stochasticity in the number and age of retired batteries available for recycling, and Wang et al. (2020) investigate a single-period deterministic setting. Both models are solved with genetic algorithms. Li et al. (2023) consider optimization of the recycling network design in a single-period model with stochasticity in material recovery rate, new battery demand, and retired battery supply. This model optimally locates facilities with fixed capacities and is solved as a two-stage MILP with second-stage decomposition.

Our work is unique in its consideration of a multi-period, stochastic, closed-loop battery recycling problem. A multi-period stochastic model motivates new approaches for generating scenarios with parameters that vary across time. Our model further chooses capacities from a continuous range, in contrast with the discrete feasible sets of other works. This approach allows for more granularity in capacity planning and expansion without making a priori assumptions on the size of constructed facilities. However, considering a continuous space of capacity decisions introduces concave cost functions due to economies of scale, making the model a nonconvex program instead of a MILP and increasing the difficulty of identifying globally optimal capacity decisions.

2.2 Linearly Constrained Concave Programming

Many important optimization problems can be formulated as a concave minimization over a polyhedron, including quadratic assignment (Bazaraa and Sherali 1982), binary programming (Raghavachari 1969), and applications with economies of scale (Feldman et al. 1966). Algorithms for globally solving concave programs date back to Tuy’s cutting planes (Tuy 1964); subsequently, a variety of branch and bound algorithms have been proposed (Rosen 1983, Benson 1985). For a survey of methods, see Pardalos and Rosen (1986) and Pardalos and Romeijn (2002).

We focus on problems with separable objective functions (i.e., representable as a sum of univariate functions). Shectman and Sahinidis (1998) propose a finitely convergent branch and bound algorithm for separable concave minimization over polyhedra, in which the feasible region is partitioned with rectangular splits and the objective is underestimated by linear functions, allowing the subproblems to be solved as linear programs. This algorithm is similar to that of Falk and Soland (1969), with improved finite convergence guarantees. D’Ambrosio et al. (2009) propose a global algorithm for separable nonconvex optimization. The algorithm splits each nonconvex function into convex and concave segments and approximates the concave segments by piecewise linear under-approximators. The approximation is solved globally as a mixed-integer convex program, and the under-approximators of the convex pieces are updated at the incumbent iterate. This algorithm converges in the limit to a global optimum. Magnanti and Stratila (2004) show approximate equivalence between MILP and linearly constrained separable concave minimization by generating piecewise linear approximations of the concave cost functions with a number of pieces that scales linearly in the inverse of the approximation error.

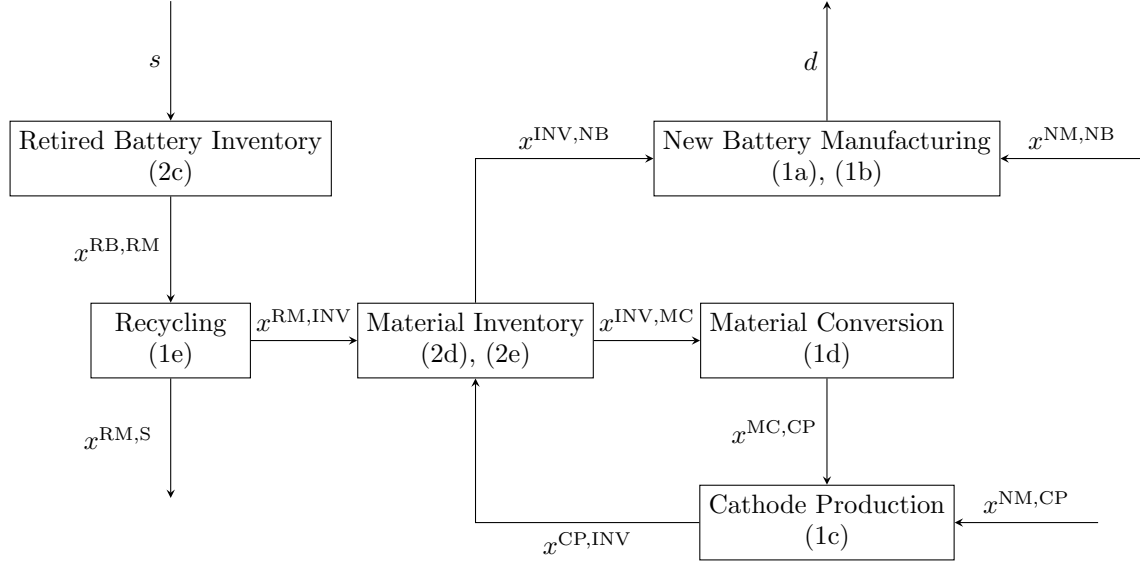


Figure 1: Material flows through the model in a single time period and location. RB represents retired batteries available for recycling, INV materials in inventory, RM recycled materials, S materials sold, and NM new materials purchased.

Our proposed algorithm solves over a sequence of piecewise linear under-approximations of the objective function, where each approximation is exact at previous iterates. As opposed to Falk and Soland (1969) and Sheftman and Sahinidis (1998), we partition on all variables simultaneously at a global optimum of the incumbent approximation. This reduces the total number of iterations, improving compatibility with iterative algorithms for decomposition. Additionally, by representing piecewise functions as MILPs, we leverage the tools, including cuts, heuristics, and branching techniques, incorporated into modern commercial solvers. D’Ambrosio et al. (2009) utilize a similar approximation and update scheme but apply the method to a broader problem class which does not admit a finite termination result.

3 EV Battery Recycling and Manufacturing Model

We model the supply chain for new EV batteries through a sequence of production steps: retired battery recycling (REC), material conversion (MC), cathode production (CP), and new battery manufacturing (NB). Figure 1 depicts the material flow through these steps. Battery recycling extracts materials from retired batteries via physical or chemical methods. If the recycling method recovers cathode powder, the cathode powder can be used directly for new battery manufacturing. Otherwise, the recycled materials are used to produce new cathode powder in the cathode production step. This step manufactures new cathode material using new or recycled precursors. Material conversion is an intermediate step to convert recycled chemicals into the compounds required as inputs for cathode production. Finally, in new battery manufacturing, EV battery cells are produced from cathode powder that is obtained from recycling or purchased from a market.

Recycling and cathode production require facilities, and facility capacities limit throughput. We assume that demand for new batteries is always satisfied, so battery manufacturing facility decisions are not included in the model. The facilities can be located in a number of zones, which model differences in facility costs by location. Zones may contain multiple facilities, and production runs in parallel across zones, with supply and demand for retired and new batteries allocated to each zone. Recycled material and retired batteries in inventory can be transported between zones.

3.1 Multistage Stochastic Battery Recycling Model

We propose a multistage stochastic optimization problem for the EV battery supply chain. The model covers two scales: a planning (strategic) scale, where facility capacity decisions are made, and an operational scale, where operational decisions, including recycling and manufacturing throughput, are made. The operational decisions respond to uncertainty in new battery demand, retired battery supply, and material cost, which is revealed progressively through a multistage scenario tree. A multistage approach ensures that the optimal solution at each period considers future uncertainty, allowing for a realistic representation of how operational decisions are made in practice.

The model time horizon spans T periods (e.g., years), with $\mathcal{T} = \llbracket T \rrbracket$. We define $\llbracket \cdot \rrbracket = \{1, \dots, \cdot\}$. The periods are partitioned into a set of L planning periods (e.g., spans of 5 years), $\mathcal{L} = \llbracket L \rrbracket$, which define the temporal granularity of the investment decisions; that is, the model allows additional capacity investment to be made at the start of each planning period. The capacity decision for a planning period constrains throughput in the time periods associated with the planning period. The set $\mathcal{T}_l \subseteq \mathcal{T}$ gives the set of time periods associated with planning period $l \in \mathcal{L}$, and, conversely, $l_t \in \mathcal{L}$ gives the planning period associated with time period $t \in \mathcal{T}$.

We separately partition the time periods \mathcal{T} into a set of S stages (e.g., spans of 10 years), $\mathcal{S} = \llbracket S \rrbracket$, which describe the points at which additional information about the stochastic parameters is revealed. The two distinct partitions of the time periods, i.e., planning periods and stages, allow for different granularity in the facility capacity solution and in the frequency that new information is revealed in the multistage scenario tree. The scenario tree has S stages, and the parameter $\sigma_t \in \mathcal{S}$ gives the stage associated with period $t \in \mathcal{T}$. Set Ω_σ contains the nodes at stage $\sigma \in \mathcal{S}$. Each node $\omega \in \Omega_\sigma$ gives a realization of the stochastic parameters (new battery demand, retired battery supply, and material cost) in the time periods associated with stage σ . A set of operational decisions in the associated periods is made at each node $\omega \in \Omega_\sigma$, in response to the realization of the stochastic parameters. For example, if each stage contains 10 years, each node gives a set of parameters for the 10 years in its stage and contains operational decisions for the same 10 years. The probability of reaching node ω in stage σ is p_ω , so $\sum_{\omega \in \Omega_\sigma} p_\omega = 1$.

To complete the description of the scenario tree, we define the paths which connect nodes to the root node of the tree. For each node ω , the function $a_\omega : \mathcal{T} \rightarrow \cup_{\sigma \in \mathcal{S}} \Omega_\sigma$ maps an input period t to the ancestor of node ω at stage σ_t . This function generalizes the parent of node ω by providing ancestors at all stages of the scenario tree. Specifically, $a_\omega(t)$ gives the node at stage σ_t which precedes ω on the unique path from the root node to node ω . If t is a period in the same stage as ω , i.e., $\omega \in \Omega_{\sigma_t}$, then $a_\omega(t) = \omega$. This function is used in the inventory balance constraints (2) to link variables which may appear in different stages. For details on our data-driven construction of a scenario tree, see Section 5.

The set of zones within the supply chain is given by \mathcal{Z} . We denote operational decisions by the variables x , which are indexed by time period $t \in \mathcal{T}$ and scenario tree node $\omega \in \Omega_{\sigma_t}$. Variables y are facility capacity decisions, which are indexed by planning period $l \in \mathcal{L}$. Specific variables are introduced in the text as they appear; additionally, tables that summarize the model variables and parameters are included in Section A.1 of the appendix.

Production

Constraints (1) model the changes between materials during new battery manufacturing, material conversion, cathode production, and battery recycling:

$$\sum_{i \in \mathcal{I}} \Delta_{i,k}^{\text{NB}} d_{\omega,z,t,i} = x_{\omega,z,t,k}^{\text{NM,NB}} + x_{\omega,z,t,k}^{\text{INV,NB}} \quad \forall k \in \mathcal{K}^{\text{CP}}, t \in \mathcal{T}, z \in \mathcal{Z}, \omega \in \Omega_{\sigma_t}, \quad (1a)$$

$$\sum_{i \in \mathcal{I}} \Delta_{i,k}^{\text{NB}} d_{\omega,z,t,i} = x_{\omega,z,t,k}^{\text{NM,NB}} \quad \forall k \in \mathcal{K} \setminus \mathcal{K}^{\text{CP}}, t \in \mathcal{T}, z \in \mathcal{Z}, \omega \in \Omega_{\sigma_t}, \quad (1b)$$

$$\sum_{k' \in \mathcal{K}^{\text{CP}}} \Delta_{k',k}^{\text{CP}} x_{\omega,z,t,k'}^{\text{CP,INV}} = x_{\omega,z,t,k}^{\text{NM,CP}} + x_{\omega,z,t,k}^{\text{MC,CP}} \quad \forall k \in \mathcal{K} \setminus \mathcal{K}^{\text{CP}}, t \in \mathcal{T}, z \in \mathcal{Z}, \omega \in \Omega_{\sigma_t}, \quad (1c)$$

$$\sum_{k' \in \mathcal{K} \setminus \mathcal{K}^{\text{CP}}} \Delta_{k',k}^{\text{MC}} x_{\omega,z,t,k'}^{\text{MC,CP}} = x_{\omega,z,t,k}^{\text{INV,MC}} \quad \forall k \in \mathcal{K} \setminus \mathcal{K}^{\text{CP}}, t \in \mathcal{T}, z \in \mathcal{Z}, \omega \in \Omega_{\sigma_t}, \quad (1d)$$

$$x_{\omega,z,t,k}^{\text{RM,INV}} + x_{\omega,z,t,k}^{\text{RM,S}} = \sum_{i \in \mathcal{I}, j \in \mathcal{J}} \Delta_{k,i,j}^{\text{REC}} x_{\omega,z,t,i,j}^{\text{RB,RM}} \quad \forall k \in \mathcal{K}, t \in \mathcal{T}, z \in \mathcal{Z}, \omega \in \Omega_{\sigma_t}. \quad (1e)$$

We remind that the process dynamics represented in constraints (1) are depicted in Figure 1. The set \mathcal{K} gives the set of materials tracked across the production processes, such as graphite, copper, and carbon black. The set of battery chemistries is given by \mathcal{I} , including chemistries of types NMC, NCA, and LFP. Cathode powders are given by the set $\mathcal{K}^{\text{CP}} \subset \mathcal{K}$. New batteries are manufactured from new or recycled cathode powder (1a) and other non-recycled new materials (e.g., graphite, aluminum) (1b) to meet battery demand $d_{\omega,z,t,i}$ for each chemistry and zone. Variables $x_{\omega,z,t,k}^{\text{NM,NB}}$ and $x_{\omega,z,t,k}^{\text{INV,NB}}$ give the mass of new and recycled material k , respectively, used in new battery production, and the parameter $\Delta_{i,k}^{\text{NB}}$ gives the amount of material k needed to manufacture a unit mass of battery with chemistry i . Equation (1c) models the production of cathode powder from new or recycled materials, where the variables $x_{\omega,z,t,k}^{\text{NM,CP}}$ and $x_{\omega,z,t,k}^{\text{MC,CP}}$ give the mass of new and recycled material inputs to cathode production, respectively. Output from cathode production is given by the variable $x_{\omega,z,t,k}^{\text{CP,INV}}$. Recycled materials used in cathode production first undergo material conversion, modeled by (1d). Inputs to material conversion are given by variable $x_{\omega,z,t,k}^{\text{INV,MC}}$ and outputs by $x_{\omega,z,t,k}^{\text{MC,CP}}$. The mass of material k required to manufacture a unit of material k' in cathode production and material conversion are given by parameters $\Delta_{k',k}^{\text{CP}}$ and $\Delta_{k',k}^{\text{MC}}$, respectively. Finally, the battery recycling processes are modeled by (1e). The set \mathcal{J} gives the available recycling processes (pyrometallurgical, hydrometallurgical, and direct), variable $x_{\omega,z,t,i,j}^{\text{RB,RM}}$ tracks the mass of batteries of chemistry i recycled with process j , and $\Delta_{k,i,j}^{\text{REC}}$ gives the amount of material k recovered per unit of recycled battery with chemistry i when using process j . The output materials can be placed into inventory to be used in manufacturing or sold to the market, modeled by variables $x_{\omega,z,t,k}^{\text{RM,INV}}$ and $x_{\omega,z,t,k}^{\text{RM,S}}$, respectively.

Inventory Balance

Constraints (2) model the flow of retired batteries and recycled materials between inventory and production processes:

$$x_{\omega,z,0,i}^{\text{RB}} = 0 \quad \forall i \in \mathcal{I}, z \in \mathcal{Z}, \omega \in \Omega_{\sigma_0}, \quad (2a)$$

$$x_{\omega,z,0,k}^{\text{INV}} = 0 \quad \forall k \in \mathcal{K}, z \in \mathcal{Z}, \omega \in \Omega_{\sigma_0}, \quad (2b)$$

$$x_{\omega,z,t,i}^{\text{RB}} = x_{\omega',z,t-1,i}^{\text{RB}} + \sum_{z' \in \mathcal{Z} \setminus \{z\}} \left(x_{\omega,z',z,t,i}^{\text{TR,RB}} - x_{\omega,z,z',t,i}^{\text{TR,RB}} \right) + s_{\omega,z,t,i} - \sum_{j \in \mathcal{J}} x_{\omega,z,t,i,j}^{\text{RB,RM}} \quad (2c)$$

$$\forall i \in \mathcal{I}, t \in \mathcal{T}, z \in \mathcal{Z}, \omega \in \Omega_{\sigma_t}, \omega' = a_{\omega}(t-1),$$

$$x_{\omega,z,t,k}^{\text{INV}} = x_{\omega',z,t-1,k}^{\text{INV}} + \sum_{z' \in \mathcal{Z} \setminus \{z\}} \left(x_{\omega,z',z,t,k}^{\text{TR,RM}} - x_{\omega,z,z',t,k}^{\text{TR,RM}} \right) + x_{\omega,z,t,k}^{\text{RM,INV}} - x_{\omega,z,t,k}^{\text{INV,MC}} \quad (2d)$$

$$\forall k \in \mathcal{K} \setminus \mathcal{K}^{\text{CP}}, t \in \mathcal{T}, z \in \mathcal{Z}, \omega \in \Omega_{\sigma_t}, \omega' = a_{\omega}(t-1),$$

$$x_{\omega,z,t,k}^{\text{INV}} = x_{\omega',z,t-1,k}^{\text{INV}} + \sum_{z' \in \mathcal{Z} \setminus \{z\}} \left(x_{\omega,z',z,t,k}^{\text{TR,RM}} - x_{\omega,z,z',t,k}^{\text{TR,RM}} \right) + x_{\omega,z,t,k}^{\text{RM,INV}} + x_{\omega,z,t,k}^{\text{CP,INV}} - x_{\omega,z,t,k}^{\text{INV,NB}} \quad (2e)$$

$$\forall k \in \mathcal{K}^{\text{CP}}, t \in \mathcal{T}, z \in \mathcal{Z}, \omega \in \Omega_{\sigma_t}, \omega' = a_{\omega}(t-1).$$

The mass of retired batteries with chemistry i in inventory is given by variable $x_{\omega,z,t,i}^{\text{RB}}$, and inventory for material k is given by $x_{\omega,z,t,k}^{\text{INV}}$. The variables $x_{\omega,z,z',t,k}^{\text{TR,RM}}$ and $x_{\omega,z,z',t,i}^{\text{TR,RB}}$ represent the transport of material k and of batteries with chemistry i , respectively, from zone z to zone z' . Constraints (2a)-(2b) enforce that initial inventory is zero. Retired

battery conservation across time periods is modeled by (2c), where the mass of newly retired batteries is given by $s_{\omega,z,t,i}$, and batteries leave inventory to be recycled. Flow balance for materials is modeled by (2d)-(2e), where material enters inventory from battery recycling or cathode production and is removed for material conversion and new battery production. Constraints (2c)-(2e) establish conservation of material across time periods, and therefore need to enforce inventory balance across stage boundaries in the multistage scenario tree. Interactions across nodes and stages are handled exclusively by these constraints.

Capacity

Constraints (3) model recycling and cathode production facility capacities:

$$\sum_{n \in \mathcal{N}_l^{\text{REC}}} y_{z,l,j,n}^{\text{REC}} \geq \sum_{i \in \mathcal{I}} x_{\omega,z,t,i,j}^{\text{RB,RM}} \quad \forall j \in \mathcal{J}, l \in \mathcal{L}, t \in \mathcal{T}_l, z \in \mathcal{Z}, \omega \in \Omega_{\sigma_t}, \quad (3a)$$

$$\sum_{n \in \mathcal{N}_{l,k}^{\text{CP}}} y_{z,l,k,n}^{\text{CP}} \geq x_{\omega,z,t,k}^{\text{CP,INV}} \quad \forall k \in \mathcal{K}^{\text{CP}}, l \in \mathcal{L}, t \in \mathcal{T}_l, z \in \mathcal{Z}, \omega \in \Omega_{\sigma_t}, \quad (3b)$$

$$\sum_{n \in \mathcal{N}_l^{\text{REC}}} y_{z,l,j,n}^{\text{REC}} \geq \sum_{n \in \mathcal{N}_{l-1}^{\text{REC}}} y_{z,l-1,j,n}^{\text{REC}} \quad \forall j \in \mathcal{J}, l \in \mathcal{L} \setminus \{1\}, z \in \mathcal{Z}, \quad (3c)$$

$$\sum_{n \in \mathcal{N}_{l,k}^{\text{CP}}} y_{z,l,k,n}^{\text{CP}} \geq \sum_{n \in \mathcal{N}_{l-1,k}^{\text{CP}}} y_{z,l-1,k,n}^{\text{CP}} \quad \forall k \in \mathcal{K}^{\text{CP}}, l \in \mathcal{L} \setminus \{1\}, z \in \mathcal{Z}, \quad (3d)$$

$$y_{z,l,j,n}^{\text{REC}} \leq u^{\text{REC}} \quad \forall j \in \mathcal{J}, l \in \mathcal{L}, z \in \mathcal{Z}, n \in \mathcal{N}_l^{\text{REC}}, \quad (3e)$$

$$y_{z,l,k,n}^{\text{CP}} \leq u^{\text{CP}} \quad \forall k \in \mathcal{K}^{\text{CP}}, l \in \mathcal{L}, z \in \mathcal{Z}, n \in \mathcal{N}_{l,k}^{\text{CP}}. \quad (3f)$$

Capacity decisions are made by planning period, so the facility capacity in planning period l applies to all scenarios and time periods \mathcal{T}_l within the planning period. Recycling capacity can be constructed at up to N_l^{REC} identical facilities within each zone, where $\mathcal{N}_l^{\text{REC}} = \llbracket N_l^{\text{REC}} \rrbracket$ is the facility index set. Variable $y_{z,l,j,n}^{\text{REC}}$ gives the capacity for facility n by recycling process j , zone z , and planning period l . Similarly, cathode production capacity is constructed on up to $N_{l,k}^{\text{CP}}$ lines, where different cathode powders are manufactured on distinct lines. The set $\mathcal{N}_{l,k}^{\text{CP}} = \llbracket N_{l,k}^{\text{CP}} \rrbracket$ gives the line indices for each cathode powder type. Variable $y_{z,l,k,n}^{\text{CP}}$ gives the capacity of line n producing cathode powder k . Constraint (3a) limits the throughput of each recycling process by the total capacity across all facilities. Similarly, cathode production throughput is constrained by (3b). Constraints (3c) and (3d) require that total capacity is nondecreasing across planning periods. Finally, recycling facilities and cathode production lines have maximum capacities of u^{REC} and u^{CP} , respectively, enforced by (3e) and (3f).

Cost

Costs related to the production process are modeled by equations (4):

$$\begin{aligned} C_{\omega,t}^{\text{OP}}(x) = & \sum_{z \in \mathcal{Z}} \left(\sum_{k \in \mathcal{K}} c_{\omega,t,k}^{\text{NB,NM}} x_{\omega,z,t,k}^{\text{NM,NB}} + \sum_{k \in \mathcal{K} \setminus \mathcal{K}^{\text{CP}}} \left(c_{\omega,t,k}^{\text{CP,NM}} x_{\omega,z,t,k}^{\text{NM,CP}} + c_{\omega,z,t,k}^{\text{MC}} x_{\omega,z,t,k}^{\text{MC,CP}} \right) \right. \\ & + \sum_{k \in \mathcal{K}} v_{\omega,t,k} \cdot \left(\rho x_{\omega,z,t,k}^{\text{INV}} - \eta x_{\omega,z,t,k}^{\text{RM,S}} \right) + \sum_{k \in \mathcal{K}^{\text{CP}}} c_{\omega,z,t,k}^{\text{CP}} x_{\omega,z,t,k}^{\text{CP,INV}} + \sum_{i \in \mathcal{I}, j \in \mathcal{J}} c_{\omega,z,t,i,j}^{\text{REC}} x_{\omega,z,t,i,j}^{\text{RB,RM}} \\ & \left. + \sum_{z' \in \mathcal{Z} \setminus \{z\}} \left(\sum_{k \in \mathcal{K}} c_{z,z'}^{\text{TR,RM}} x_{\omega,z,z',t,k}^{\text{TR,RM}} + \sum_{i \in \mathcal{I}} c_{z,z'}^{\text{TR,RB}} x_{\omega,z,z',t,i}^{\text{TR,RB}} \right) \right) \quad \forall t \in \mathcal{T}, \omega \in \Omega_{\sigma_t}, \end{aligned} \quad (4a)$$

$$C_t^{\text{PL}}(y) = \sum_{z \in \mathcal{Z}} \left(\sum_{j \in \mathcal{J}} \sum_{n \in \mathcal{N}_{l_t}^{\text{REC}}} f_{z,j}^{\text{REC}}(y_{z,l_t,j,n}^{\text{REC}}) + \sum_{k \in \mathcal{K}^{\text{CP}}} \sum_{n \in \mathcal{N}_{l_t,k}^{\text{CP}}} f_{z,k}^{\text{CP}}(y_{z,l_t,k,n}^{\text{CP}}) \right) \quad \forall t \in \mathcal{T}. \quad (4b)$$

Operational costs per time period, including material, utility, transportation, and inventory costs, as well as revenue incurred by selling recycled material, are linear functions of operational decisions x and are represented by the functions $C_{\omega,t}^{\text{OP}}(x)$, defined in (4a). The parameters $c_{\omega,t,k}^{\text{NB,NM}}$ and $c_{\omega,t,k}^{\text{CP,NM}}$ give the purchase costs per unit of new material k used in new battery manufacturing and cathode production, respectively. The variable costs of producing a unit of material k via material conversion, manufacturing a unit of cathode powder k via cathode production, and recycling a unit of batteries of chemistry i via process j are given by $c_{\omega,z,t,k}^{\text{MC}}$, $c_{\omega,z,t,k}^{\text{CP}}$, and $c_{\omega,z,t,i,j}^{\text{REC}}$, respectively. Per-unit transportation costs from zone z to zone z' are given by $c_{z,z'}^{\text{TR,RM}}$ for materials and $c_{z,z'}^{\text{TR,RB}}$ for batteries. The revenue generated per unit of recycled material k sold is a proportion $\eta \leq 1$ of the value of the material $v_{\omega,t,k}$; selling extraneous recycled materials that are not used in downstream manufacturing helps offset recycling facility costs. Inventory costs are similarly incurred as a proportion ρ of the value of material held in inventory. We note that stochastic parameters are indexed by node ω .

Planning costs include capital and labor costs, and are represented by the functions $C_t^{\text{PL}}(y)$, defined in (4b). Capital costs include costs for facility construction and equipment purchases. These costs are concave functions due to economies of scale (Dai et al. 2019). Planning costs are defined in terms of functions f , where $f_{z,j}^{\text{REC}}(y_{z,l_t,j,n}^{\text{REC}})$ gives the long-term costs of facilities by recycling process and zone, and $f_{z,k}^{\text{CP}}(y_{z,l_t,k,n}^{\text{CP}})$ those of a cathode production line producing material k . The functions $f : \mathbb{R}_+ \rightarrow \mathbb{R}$ are concave lower semicontinuous piecewise with the form

$$f(y) = \begin{cases} \sum_i q_i y^{r_i} + w & y > 0 \\ 0 & y = 0. \end{cases} \quad (5)$$

The functions introduce a cost of 0 when no capacity is constructed, and otherwise are the sum of concave power terms ($r_i \in (0, 1]$ and $q_i \geq 0$) and a constant term ($w \geq 0$), and thus are monotonic increasing.

Complete Model

We seek to minimize total expected costs over the model horizon with an annual discount factor of γ , subject to the constraint logic presented in this section:

$$\begin{aligned} \min_{x,y} \quad & \sum_{t \in \mathcal{T}} (1 - \gamma)^{t-1} \left(C_t^{\text{PL}}(y) + \sum_{\omega \in \Omega_{\sigma_t}} p_{\omega} C_{\omega,t}^{\text{OP}}(x) \right) \\ \text{s.t.} \quad & (1), (2), (3) \\ & x \geq 0, y \geq 0. \end{aligned} \quad (\text{P})$$

The model (P) is a minimization of a separable concave function subject to linear constraints.

3.2 Model Properties

In the remainder of this paper, we assume that Assumption 1 holds. The assumption enforces reasonable characteristics on the model data, including nonnegativity of costs, values, probabilities, supply, demand, material requirements, and maximum capacities. The properties of the functions f hold by their structure (5), and discount factor γ naturally falls on $[0, 1)$.

Assumption 1. The parameters d, s, c, v, p , and Δ are nonnegative, u is positive, $\gamma \in [0, 1)$, and functions f are concave monotonic increasing with $f(0) = 0$.

Each scenario has a relatively complete recourse property, given in Proposition 1. This property ensures that, for any feasible capacity decision y , there is some feasible operational decision x . We further show in Proposition 2 that the model is feasible and has an optimal solution at an extreme point of its feasible region. These and other original proofs are provided in Section A.4 of the appendix.

Proposition 1. For any $\bar{y} \geq 0$ that satisfies (3c)-(3f), $\{(y, x) \geq 0 : (1), (2), (3), y = \bar{y}\} \neq \emptyset$.

Proposition 2. The model (P) is feasible and has an optimal solution at an extreme point of its feasible region.

For convenience of notation, we introduce the operator $\mathcal{C}(\mathcal{X}; \nu)$ which counts the number of elements of a set \mathcal{X} that take the value ν : $\mathcal{C}(\mathcal{X}; \nu) = \sum_{x \in \mathcal{X}} \mathbb{I}(x = \nu)$. In Theorem 1, we note that any extreme point of the feasible region of (P) satisfies a specific structure in the capacity decision y . Specifically, each facility is constructed to its upper bound before adding any capacity to the next facility. For a recycling solution y^{REC} with total capacity $Y_{z,l,j} := \sum_{n \in \mathcal{N}_l^{\text{REC}}} y_{z,l,j,n}^{\text{REC}}$, the structure is defined by

$$\begin{aligned} \mathcal{C}(\{y_{z,l,j,n}^{\text{REC}}\}_{n \in \mathcal{N}_l^{\text{REC}}}; u^{\text{REC}}) &\geq \left\lceil \frac{Y_{z,l,j}}{u^{\text{REC}}} \right\rceil - 1; \\ \mathcal{C}(\{y_{z,l,j,n}^{\text{REC}}\}_{n \in \mathcal{N}_l^{\text{REC}}}; 0) &\geq |\mathcal{N}_l^{\text{REC}}| - \left\lceil \frac{Y_{z,l,j}}{u^{\text{REC}}} \right\rceil \quad \forall j \in \mathcal{J}, l \in \mathcal{L}, z \in \mathcal{Z}, \end{aligned} \quad (6)$$

with a corresponding structure for $y_{z,l,k,n}^{\text{CP}}$ defined in the appendix, equation (A.3). Under this structure, there is at most one facility with capacity not equal to its upper or lower bound. As (P) has an optimal extreme point, we conclude that the model has an optimal solution with this structure.

Theorem 1. Let (\tilde{y}, \tilde{x}) be an extreme point of $\{(y, x) \geq 0 : (1), (2), (3)\}$. Then, \tilde{y}^{REC} satisfies (6) and \tilde{y}^{CP} satisfies the corresponding property.

3.3 Reformulating the Model

Under the structure of the optimal solution implied by Theorem 1, we reformulate the capacity decision variables y and associated constraints (3). In the reformulation, integer variables $y_{z,l,j}^{\text{REC}}$ and $y_{z,l,k}^{\text{CP}}$ give the number of facilities with capacities at their upper bound, and continuous variables $y_{z,l,j,+}^{\text{REC}}$ and $y_{z,l,k,+}^{\text{CP}}$ give the capacity of the single facility not at its upper or lower bound:

$$u^{\text{REC}} y_{z,l,j}^{\text{REC}} + y_{z,l,j,+}^{\text{REC}} \geq \sum_{i \in \mathcal{I}} x_{\omega,z,t,i,j}^{\text{RB,RM}} \quad \forall j \in \mathcal{J}, l \in \mathcal{L}, t \in \mathcal{T}_l, z \in \mathcal{Z}, \omega \in \Omega_{\sigma_t}, \quad (7a)$$

$$u^{\text{CP}} y_{z,l,k}^{\text{CP}} + y_{z,l,k,+}^{\text{CP}} \geq x_{\omega,z,t,k}^{\text{CP,INV}} \quad \forall k \in \mathcal{K}^{\text{CP}}, l \in \mathcal{L}, t \in \mathcal{T}_l, z \in \mathcal{Z}, \omega \in \Omega_{\sigma_t}, \quad (7b)$$

$$u^{\text{REC}} y_{z,l,j}^{\text{REC}} + y_{z,l,j,+}^{\text{REC}} \geq u^{\text{REC}} y_{z,l-1,j}^{\text{REC}} + y_{z,l-1,j,+}^{\text{REC}} \quad \forall j \in \mathcal{J}, l \in \mathcal{L} \setminus \{1\}, z \in \mathcal{Z}, \quad (7c)$$

$$u^{\text{CP}} y_{z,l,k}^{\text{CP}} + y_{z,l,k,+}^{\text{CP}} \geq u^{\text{CP}} y_{z,l-1,k}^{\text{CP}} + y_{z,l-1,k,+}^{\text{CP}} \quad \forall k \in \mathcal{K}^{\text{CP}}, l \in \mathcal{L} \setminus \{1\}, z \in \mathcal{Z}, \quad (7d)$$

$$y_{z,l,j}^{\text{REC}} \in \{0, \dots, |\mathcal{N}_l^{\text{REC}}| - 1\} \quad \forall j \in \mathcal{J}, l \in \mathcal{L}, z \in \mathcal{Z}, \quad (7e)$$

$$y_{z,l,k}^{\text{CP}} \in \{0, \dots, |\mathcal{N}_{l,k}^{\text{CP}}| - 1\} \quad \forall k \in \mathcal{K}^{\text{CP}}, l \in \mathcal{L}, z \in \mathcal{Z}, \quad (7f)$$

$$y_{z,l,j,+}^{\text{REC}} \leq u^{\text{REC}} \quad \forall j \in \mathcal{J}, l \in \mathcal{L}, z \in \mathcal{Z}, \quad (7g)$$

$$y_{z,l,k,+}^{\text{CP}} \leq u^{\text{CP}} \quad \forall k \in \mathcal{K}^{\text{CP}}, l \in \mathcal{L}, z \in \mathcal{Z}. \quad (7h)$$

We also introduce for all $t \in \mathcal{T}$ an adjusted version of the planning cost function:

$$\bar{C}_t^{\text{PL}}(y) = \sum_{z \in \mathcal{Z}} \left(\sum_{j \in \mathcal{J}} (f_{z,j}^{\text{REC}}(y_{z,l_t,j,+}^{\text{REC}}) + y_{z,l_t,j}^{\text{REC}} f_{z,j}^{\text{REC}}(u^{\text{REC}})) + \sum_{k \in \mathcal{K}^{\text{CP}}} (f_{z,k}^{\text{CP}}(y_{z,l_t,k,+}^{\text{CP}}) + y_{z,l_t,k}^{\text{CP}} f_{k,z}^{\text{CP}}(u^{\text{CP}})) \right).$$

The full reformulated model is then given by

$$\begin{aligned} \min_{x,y} \quad & \sum_{t \in \mathcal{T}} (1 - \gamma)^{t-1} \left(\bar{C}_t^{\text{PL}}(y) + \sum_{\omega \in \Omega_{\sigma_t}} p_{\omega} C_{\omega,t}^{\text{OP}}(x) \right) \\ \text{s.t.} \quad & (1), (2), (7) \\ & x \geq 0, y \geq 0. \end{aligned} \tag{PMI}$$

The new model (PMI) is equivalent to the original formulation (P), shown in Theorem 2. It also retains the linearly constrained separable concave structure of (P) with the addition of integrality constraints. Although these constraints add some complexity, the number of capacity variables is significantly reduced as they are no longer indexed by \mathcal{N}^{REC} and \mathcal{N}^{CP} .

Theorem 2. *The models (P) and (PMI) have the same optimal objective value.*

3.4 Open-Loop Models

Our model takes the perspective of closed-loop supply chain, where materials recovered from recycling are used to manufacture new batteries. The open-loop perspective instead sells the recovered materials to a market. Under the assumption that the nonnegativity constraint on $x^{\text{NM,NB}}$ (the amount of new material used in new battery production) is non-binding, $x^{\text{NM,NB}}$ can be replaced with its definition from constraint (1a). This assumption holds if the material requirements for manufacturing new batteries cannot be met through recycling alone. Then, the objective contribution from $x^{\text{NM,NB}}$ becomes

$$\sum_{z \in \mathcal{Z}, t \in \mathcal{T}, k \in \mathcal{K}^{\text{CP}}, \omega \in \Omega_{\sigma_t}} c_{\omega,t,k}^{\text{NM,NB}} x_{z,\omega,t,k}^{\text{NM,NB}} = \sum_{z \in \mathcal{Z}, t \in \mathcal{T}, k \in \mathcal{K}^{\text{CP}}, \omega \in \Omega_{\sigma_t}} c_{\omega,t,k}^{\text{NM,NB}} \left(\sum_{i \in \mathcal{I}} \Delta_{i,k}^{\text{NB}} d_{\omega,z,t,i} - x_{z,\omega,t,k}^{\text{INV,NB}} \right).$$

This change effectively removes the new battery manufacture portion of the model and adds a revenue associated with “selling” recycled cathode powder at the market price, which represents the dynamics of an open-loop recycler. In the remainder of this work, we focus on the closed-loop recycling model, although our approach, optimal solutions, and discussion generalize to an open-loop setting.

4 Algorithmic Approaches

4.1 Adaptive Piecewise Linear Approximation Algorithm

We propose a finitely convergent algorithm to find globally optimal solutions for separable concave minimization problems with linear constraints and mixed-integer variables. The algorithm under-approximates each univariate concave objective function with a piecewise linear function, optimizes over the approximation, then updates the functions by introducing breakpoints at the incumbent solution, making the approximation exact at the current iterate. The subproblem objectives provide lower bounds on the global optimum, and revisiting an iterate yields an optimality certificate.

In this section, we define new notation which is distinct from the previous section. For analysis of our algorithm, we introduce a stylized version of the models (P) and (PMI):

$$\min_{(y,x) \in \mathcal{X}} \sum_{i=1}^{n_y} f_i(y_i) + \sum_{\omega \in \Omega_1} p_\omega c_\omega^T x_\omega, \quad (\text{SCP})$$

where the feasible region is

$$\mathcal{X} = \{(y, \{x_\omega\}_{\omega \in \Omega_1}) \geq 0 : y \in \mathbb{Z}^{n_1} \times \mathbb{R}^{n_y - n_1}, Ay = b, B_\omega x_\omega + Dy = d_\omega \forall \omega \in \Omega_1\}.$$

The functions $f_i : \mathbb{R} \rightarrow \mathbb{R}$ are concave lower semicontinuous, $p_\omega \in \mathbb{R}$, $c_\omega \in \mathbb{R}^{n_x}$, $A \in \mathbb{R}^{m_1 \times n_y}$, $b \in \mathbb{R}^{m_1}$, $B_\omega \in \mathbb{R}^{m_2 \times n_x}$, $D \in \mathbb{R}^{m_2 \times n_y}$ and $d_\omega \in \mathbb{R}^{m_2}$. The number of integer capacity variables is given by n_1 . This notation emphasizes the scenario-based structure in the operational scale with blocks for each first-stage node, but generalizes the structure of descendant nodes by modeling them in the extensive form. That is, for $\omega \in \Omega_1$, the parameters $(c_\omega, B_\omega, D, d_\omega)$ contain objective and constraint data for all descendant scenarios of node ω . We assume \mathcal{X} is nonempty and bounded, so any feasible y satisfies some consistent bounds $\underline{y} \leq y \leq \bar{y}$. This assumption is reasonable as the models have finite optimal solutions by Proposition 2. We further assume a relatively complete recourse property, which holds for our models by Proposition 1:

$$\{x \geq 0 : B_\omega x = d_\omega - Dy\} \neq \emptyset \quad \forall \omega \in \Omega_1, y \in \mathbb{Z}^{n_1} \times \mathbb{R}^{n_y - n_1} : y \geq 0, Ay = b. \quad (8)$$

We now detail our algorithm. Given a set of k_i breakpoints $\{y_i^{(j)}\}_{j=1}^{k_i}$ for variable y_i ordered so that $y_i^{(j)} < y_i^{(j+1)}$, we construct piecewise linear functions $\bar{f}_i : [y_i^{(1)}, y_i^{(k_i)}] \rightarrow \mathbb{R}$ by

$$\bar{f}_i(y_i) = \begin{cases} \frac{f_i(y_i^{(j+1)}) - f_i(y_i^{(j)})}{y_i^{(j+1)} - y_i^{(j)}}(y_i - y_i^{(j)}) + f_i(y_i^{(j)}) & y_i \in [y_i^{(j)}, y_i^{(j+1)}] \quad \forall j \in \llbracket k_i - 1 \rrbracket. \end{cases} \quad (9)$$

We build a subproblem (SP) that replaces the objective of (SCP) with the piecewise functions \bar{f}_i :

$$\min_{(y,x) \in \mathcal{X}} \sum_{i=1}^n \bar{f}_i(y_i) + \sum_{\omega \in \Omega_1} p_\omega c_\omega^T x_\omega. \quad (\text{SP})$$

As \bar{f}_i are underestimators of f_i , the subproblems are relaxations of (SCP). The piecewise functions can be modeled with SOS-2 constraints or mixed-integer variables.

Denote the (polyhedral) set formed by fixing the discrete variables of \mathcal{X} to some solution \bar{y} by $\mathcal{X}(\bar{y}) = \{(y, x) \in \mathcal{X} : y_i = \bar{y}_i \forall i \in \llbracket n_1 \rrbracket\}$. Lemma 1 shows that there is an optimal solution for (SP) that falls at an extreme point of $\mathcal{X}(y^*)$ for some y^* .

Lemma 1. *Let $(y^*, x^*) \in \mathcal{X}$ be an optimal solution to (SP). Then, there is an optimal solution that is an extreme point of $\mathcal{X}(y^*)$.*

Assumption 2. *Solving (SP) yields an optimal solution (y^*, x^*) that is an extreme point of $\mathcal{X}(y^*)$.*

We propose the adaptive piecewise linear approximation algorithm (aPWL), Algorithm 1, that solves a sequence of subproblems (SP) and updates the breakpoints defining the piecewise functions at every iteration. As the subproblems minimize piecewise linear functions subject to linear and integrality constraints, they can be solved to global optimality via an LP-based branch and bound solver. Assumption 2 establishes that solving (SP) in step 3 yields one of the optimal extreme points described in Lemma 1. A branch and bound solver can be tailored to

Algorithm 1: Adaptive Piecewise Linear Approximation

- 1 Initialize $(y_i^{(1)}, y_i^{(2)}) \leftarrow (y_i, \bar{y}_i)$ and $k_i \leftarrow 2 \quad \forall i \in \llbracket n_y \rrbracket$. Set $s \leftarrow 1$.
 - 2 For all $i \in \llbracket n_y \rrbracket$, construct \bar{f}_i^s by (9) with breakpoints $\{y_i^{(j)}\}_{j=1}^{k_i}$.
 - 3 Solve $\min_{(y,x) \in \mathcal{X}} \sum_{i=1}^n \bar{f}_i^s(y_i) + \sum_{\omega \in \Omega_1} p_\omega c_\omega^T x_\omega$ to optimal solution $(\tilde{y}^s, \{\tilde{x}_\omega^s\}_{\omega \in \Omega_1})$.
 - 4 If $\bar{f}_i^s(\tilde{y}_i^s) \geq f_i(\tilde{y}_i^s)$ for all i , STOP, $(\tilde{y}^s, \{\tilde{x}_\omega^s\}_{\omega \in \Omega_1})$ is optimal for (SCP).
 - 5 Otherwise, for each i where $\bar{f}_i^s(\tilde{y}_i^s) < f_i(\tilde{y}_i^s)$, add breakpoint $y_i^{(k_i+1)} \leftarrow \tilde{y}_i^s$. Set $k_i \leftarrow k_i + 1$. Reindex $\{y_i^{(j)}\}_{j=1}^{k_i}$ so that $y_i^{(j)} < y_i^{(j+1)}$ for all $i \in \llbracket n_y \rrbracket$ and $j \in \llbracket k_i - 1 \rrbracket$.
 - 6 Set $s \leftarrow s + 1$. Go to 2.
-

generate optimal extreme points of the restricted feasible region, satisfying this assumption. Under Assumption 2, the algorithm converges finitely to a global optimum of (SCP), shown in Theorem 3.

Theorem 3. *Algorithm 1 terminates finitely with a global optimum of (SCP).*

4.2 Scale Decomposition

We further leverage the multistage stochastic structure of the model by employing a Benders' decomposition scheme (Benders 1962) in step 3 of Algorithm 1 that separates decisions at the planning scale from those at the operational scale. In the context of stochastic optimization, this decomposition is also referred to as the L-shaped method (Van Slyke and Wets 1969). The subproblems (SP) are solved iteratively by generating cuts from the operational scale. The operational problem is separable over the first-stage nodes Ω_1 and thus can be solved in parallel as linear programs. We do not further decompose over nodes at later stages in the multistage scenario tree; experiments on this style of decomposition (i.e., the nested L-shaped method, see Birge and Louveaux 2011, Ch. 6.1) do not reduce computation times for the size of problem considered in this work. Importantly, every scenario has a relatively complete recourse property (8), so the decomposition scheme does not need to add cuts that enforce feasibility.

For each operational problem indexed by $\omega \in \Omega_1$, we denote the extreme points of the dual feasible region $\{\pi : p_\omega c_\omega \geq B_\omega^T \pi\}$ by $\pi_j^{(\omega)}$ for $j \in \mathcal{J}_\omega$, where \mathcal{J}_ω is an index set for the dual extreme points of problem ω . Under property (8), every operational problem has a finite optimal solution for any capacity decision y . Thus, each dual problem has a finite optimum at some extreme point $\pi_j^{(\omega)}$. The dual problems can then be equivalently represented by the convex piecewise linear value functions

$$v_\omega(y) = \max_{j \in \mathcal{J}_\omega} (d_\omega - Dy)^T \pi_j^{(\omega)}. \quad (10)$$

The Benders' decomposition approximates v_ω by adding valid cuts at incumbent capacity solutions y . Importantly, added cuts remain valid between iterations of Algorithm 1, allowing warmstarting of the decomposition between iterations and decreasing the number of new cuts required to converge.

For the sake of computational efficiency, we only partially decompose the operational problems. We construct groups of first-stage nodes and apply the Benders' cut generation approach to each group. This approach is similar to that employed by Adulyasak et al. (2015). Let the groups $\{\mathcal{G}_e\}_{e=1}^{n_g}$ be a partition of the nodes Ω_1 . Then, we generate cuts for the grouped value functions

$$\max_{\{j_\omega\}_{\omega \in \mathcal{G}_e} \in \prod_{\omega \in \mathcal{G}_e} \mathcal{J}_\omega} \sum_{\omega \in \mathcal{G}_e} (d_\omega - Dy)^T \pi_{j_\omega}^{(\omega)}, \quad (11)$$

instead of the individual functions (10). Grouping in such a way reduces the number of convex functions to model but increases the number of linear pieces in each function. We describe how the groups $\{\mathcal{G}_e\}_{e=1}^{n_g}$ are chosen in Section 5.3.

5 Data Sources and Scenario Generation

We model the recycling and manufacture of six battery chemistries: NMC(111), NMC(532), NMC(622), NMC(811), NCA, and LFP. NMC are lithium nickel manganese cobalt oxides, NCA is a lithium nickel cobalt aluminum oxide, and LFP is lithium iron phosphate. Batteries can be recycled through pyrometallurgical, hydrometallurgical, or direct processes. The time horizon covers 2021 to 2050 with annual granularity, and planning periods are the six 5-year intervals: 2021-2025, 2026-2030, 2031-2035, 2036-2040, 2041-2045, and 2046-2050. The stages of the multistage scenario tree are the three 10-year intervals: 2021-2030, 2031-2040, and 2041-2050.

Deterministic parameters are computed using the extensive low-level formulas and high-fidelity data from the EverBatt model (Dai et al. 2019). The parameters Δ , u , f , $c^{\text{TR,RM}}$, and $c^{\text{TR,RB}}$ are derived from EverBatt. We take a discount rate $\gamma = 3\%$ to match the Federal Energy Management Program discount rate for 2021 (Kneifel and Webb 2020). Inventory costs are set as $\rho = 25\%$ of material value (Azzi et al. 2014), and we assume that $\eta = 70\%$ of material value is recovered when selling recycled materials to the market.¹

The numbers of recycling facilities and cathode production lines are determined by the number of facilities and lines needed to recycle the largest annual retired battery supply and to manufacture cathode powder to satisfy the largest annual new battery demand during each planning period:

$$|\mathcal{N}_t^{\text{REC}}| = \left\lceil \frac{1}{u^{\text{REC}}} \max_{t \in \mathcal{T}_1} \max_{\omega \in \Omega_{\sigma_t}} \sum_{i \in \mathcal{I}, z \in \mathcal{Z}} s_{\omega,z,t,i} \right\rceil \quad \text{and} \quad |\mathcal{N}_{l,k}^{\text{CP}}| = \left\lceil \frac{1}{u^{\text{CP}}} \max_{t \in \mathcal{T}_1} \max_{\omega \in \Omega_{\sigma_t}} \sum_{i \in \mathcal{I}, z \in \mathcal{Z}} \Delta_{i,k}^{\text{NB}} d_{\omega,z,t,i} \right\rceil,$$

where the maximum capacities from EverBatt are $u^{\text{REC}} = 100,000$ tonnes/year and $u^{\text{CP}} = 2,000$ tonnes/year (Dai et al. 2019).

5.1 Battery Supply and Demand Scenarios

We follow the methodology and data from Xu et al. (2020) for constructing deterministic global EV stock projections under the International Energy Agency’s Sustainable Development Scenario (SDS) and Stated Policies Scenario (STEPS) (IEA 2020). The projections give the total number of active EVs (EV *stock*), including battery and plug-in hybrid EVs, in each year over the 30-year period from 2021 to 2050. We label these two projections EV_t^{SDS} and EV_t^{STEPS} . Time periods are standardized, so $t = 1$ corresponds to 2021 and $T = 30$ to 2050. The parameter $EV_0 = EV_0^{\text{SDS}} = EV_0^{\text{STEPS}}$ gives the measured number of active EVs in 2020.

We denote the year-over-year rate of change in EV stock under the two projections by $\delta_t^{\text{EV,SDS}}$ and $\delta_t^{\text{EV,STEPS}}$, e.g., $\delta_t^{\text{EV,SDS}} = EV_t^{\text{SDS}}/EV_{t-1}^{\text{SDS}}$. Let δ_t^{EV} be the random variable that represents the rate of change in EV stock for year t . We define the distribution of δ_t^{EV} by

$$\delta_t^{\text{EV}} = \frac{1}{2} \left| \delta_t^{\text{EV,SDS}} - \delta_t^{\text{EV,STEPS}} \right| Z_{\sigma_t}^{\text{EV}} + \frac{1}{2} \left(\delta_t^{\text{EV,SDS}} + \delta_t^{\text{EV,STEPS}} \right),$$

where the randomness is described by a random variable Z_{σ}^{EV} for each stage $\sigma \in \mathcal{S}$. We assume that these random variables are distributed as truncated standard normals on the interval $[-2, 2]$ and are independent across stages.

We generate a discrete distribution by approximating Z_{σ}^{EV} with n_d values via Gaussian quadrature (Miller III and Rice 1983). For each index $\xi_{\sigma} \in \llbracket n_d \rrbracket$, Gaussian quadrature produces an observation of Z_{σ}^{EV} , labeled $\bar{Z}_{\xi_{\sigma}}^{\text{EV}}$, and a corresponding probability $p_{\xi_{\sigma}}^{\text{EV}}$. Gaussian quadrature guarantees that the first $2n_d - 1$ moments of the discrete

distributions match those of the underlying truncated normal distributions. We convert the observations $\bar{Z}_{\xi\sigma}^{\text{EV}}$ into a set of multistage demand scenarios by considering combinations of observations across stages, i.e., taking the cartesian product over S copies of the observations. The multistage index is some $\xi \in \llbracket n_d \rrbracket^S$, and the corresponding time series for the observations of the rate of change in EV stock, denoted $\{\delta_{\xi,t}^{\text{EV}}\}_{t \in \mathcal{T}}$, are computed by

$$\delta_{\xi,t}^{\text{EV}} = \frac{1}{2} \left| \delta_t^{\text{EV,SDS}} - \delta_t^{\text{EV,STEPS}} \right| \bar{Z}_{\xi\sigma_t}^{\text{EV}} + \frac{1}{2} \left(\delta_t^{\text{EV,SDS}} + \delta_t^{\text{EV,STEPS}} \right).$$

Then, the EV stock observations for the demand scenario, labeled $EV_{\xi,t}$ are given by

$$EV_{\xi,t} = EV_0 \prod_{t'=1}^t \delta_{\xi,t'}^{\text{EV}}.$$

This approach relies on the independence of Z_{σ}^{EV} across stages, which implies the independence of the rate of change δ_t^{EV} in different stages. However, the observations of EV stock are not independent across stages, as they depend on the history of the random variable δ_t^{EV} . Each observation $EV_{\xi,t}$ only depends on the realization of $\bar{Z}_{\sigma}^{\text{EV}}$ at the current or prior stages, which is consistent with how information is revealed over stages of a scenario tree.

We next separate the number of active EV batteries by age. Using data from Xu et al. (2020), we designate LS_a as the percentage of batteries of age a that retire at their current age, with a maximum lifespan of A . Denote by $AB_{\xi,t,a}$ the number of active batteries in year t , demand scenario ξ that are a years old. The parameter $AB_{\xi,t,a}$ is computed recursively,

$$AB_{\xi,t,a} = \begin{cases} (1 - LS_a) AB_{\xi,t-1,a-1} & a > 0 \\ \left[EV_{\xi,t} - EV_{\xi,t-1} + \sum_{a'=1}^A LS_{a'} AB_{\xi,t-1,a'-1} \right]^+ & a = 0 \end{cases} \quad \forall \xi \in \llbracket n_d \rrbracket^S, t \in \mathcal{T}, a \in \{0, \dots, A\},$$

where $[\cdot]^+ = \max\{\cdot, 0\}$. By this definition, the number of new ($a = 0$) batteries is the sum of the year-over-year increase in active batteries and the number of retired batteries, and older ($a > 0$) batteries are reduced by the retirement proportion LS_a as they age. The initial state $AB_{\xi,0,a}$ is taken from historical data (IEA 2020, 2023).

We convert from battery counts to mass and split by cathode chemistry, distinguishing between two projections for market shares of battery chemistries. Xu et al. (2020) also provide these projections: in the first (the NCX projection), NMC chemistries are more prominent, and in the second (the LFP projection), LFP chemistries are more prominent. We label these market share projections $MS_{\text{NCX},t,i}$ and $MS_{\text{LFP},t,i}$, representing the proportion of new battery sales that are of chemistry i by year and projection. These parameters include historical data through year $-A$. We now index by market share projection and EV stock observation: $(\psi, \xi) \in \{\text{NCX}, \text{LFP}\} \times \llbracket n_d \rrbracket^S$. To account for changes in average battery size due to differences in battery EV (BEV) and plug-in hybrid (PHEV) adoption, we compute an additional parameter $m_{\xi,t,i}$, representing the average mass of a new battery by chemistry. The computation of $m_{\xi,t,i}$ is described in Section A.2 of the appendix.

Supply and demand for new batteries by chemistry is then given, respectively, by

$$s_{(\psi,\xi),z,t,i} = \beta_z m_{\xi,t,i} \sum_{a=1}^A MS_{\psi,t-a,i} LS_a AB_{\xi,t-1,a-1} \quad \text{and} \quad d_{(\psi,\xi),z,t,i} = \beta_z m_{\xi,t,i} MS_{\psi,t,i} AB_{\xi,t,0},$$

where $\beta_z \in (0, 1]$ is a scale parameter that gives the proportion of the global EV market allocated to each zone z . Figure 2 shows a set of supply and demand scenarios generated with this method.

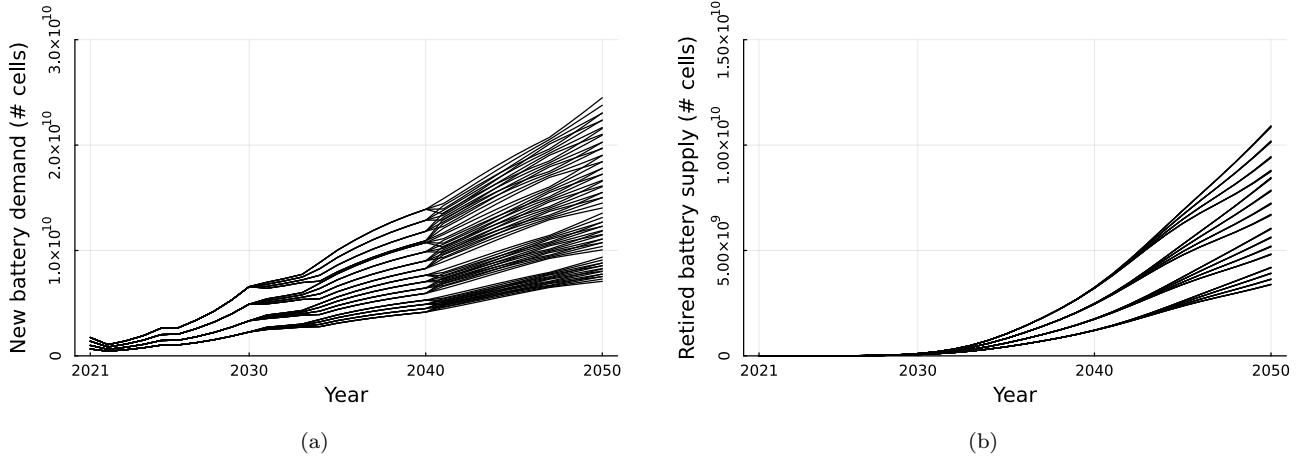


Figure 2: A set of three-stage ($S = 3$) new battery demand (a) and recycled battery supply (b) scenarios for chemistry NMC(622) with $n_d = 4$ and $\beta = 1$.

5.2 Cost Scenarios

We assume that changes in cost coefficients are due to fluctuations in the value of “critical minerals”: copper (Cu), cobalt (Co), lithium (Li), manganese (Mn), and nickel (Ni). Let $\mathcal{M} = \{\text{Cu}, \text{Co}, \text{Li}, \text{Mn}, \text{Ni}\}$ be this set of metals. From this assumption, only material costs and values vary by scenario and time; all other costs are static at the values from EverBatt.

To account for correlations between EV demand and metal prices, we construct n_c cost scenarios for each demand scenario $(\psi, \xi) \in \{\text{NCX}, \text{LFP}\} \times \llbracket n_d \rrbracket^S$. We leverage metal price projections from Boer et al. (2024), who construct forecasts in line with the assumptions of the SDS and STEPS projections. For each metal, this work fits a vector autoregressive model to predict metal production and metal price. The regression depends on three randomly distributed exogenous shocks to the metal market, namely, an aggregate demand shock, a metal-specific demand shock, and a metal supply shock. Following the approach of Antolín-Díaz et al. (2021), a conditional distribution of the future metal price time series is estimated by a sampling algorithm, where the distribution is conditioned so that predicted metal production matches the projected values from SDS or STEPS and the aggregate demand and metal supply shocks follow their unconditional distributions. Effectively, this conditional distribution is of predicted metal prices that result from a series of metal demand shocks that generate the projected metal production levels from SDS or STEPS. From these results, we take for each metal an annual median price estimate and a 40% highest posterior density (HPD) region under each of the SDS and STEPS projections from 2020 to 2040 (Boer et al. 2024, Fig. 4).² The data is extended to 2050 by setting the values for years 2041-2050 to the value from 2040. Let $v_{t,m}^{\text{MED},\text{SDS}}$ and $v_{t,m}^{\text{MED},\text{STEPS}}$ be the median estimates for each projection, and $[v_{t,m}^{\text{LB},\text{SDS}}, v_{t,m}^{\text{UB},\text{SDS}}]$ and $[v_{t,m}^{\text{LB},\text{STEPS}}, v_{t,m}^{\text{UB},\text{STEPS}}]$ be the HPD intervals for each metal m .

As demand and cost data are associated with the same underlying International Energy Agency projections (i.e., SDS and STEPS), we use the relationship between demand scenarios and the projections to produce a set of scenario-adjusted cost distribution parameters. First, we characterize each demand scenario by a multiplier

$$\lambda_{\xi,t} = \text{proj}_{[0,1]} \left(\frac{EV_{\xi,t} - EV_t^{\text{STEPS}}}{EV_t^{\text{SDS}} - EV_t^{\text{STEPS}}} \right).$$

This multiplier characterizes in each year how similar the EV stock realization is to the SDS and STEPS projections, where values near 1 imply similarity to SDS and values near 0 similarity to STEPS. We compute the scenario-

adjusted distribution parameters $v_{\xi,t,m}^{\text{MED}}$, $v_{\xi,t,m}^{\text{LB}}$, and $v_{\xi,t,m}^{\text{UB}}$ from these multipliers, e.g.,

$$v_{\xi,t,m}^{\text{MED}} = v_{\xi,t,m}^{\text{MED,SDS}} \lambda_{\xi,t} + v_{\xi,t,m}^{\text{MED,STEPS}} (1 - \lambda_{\xi,t}).$$

Under this formula, for demand scenarios that are closer to the SDS projection than STEPS, the cost distribution parameters are also closer to their SDS counterpart. This introduces reasonable relationships between EV demand and metal prices.

Let $v_{\xi,t,m}$ be the random variable that represents the price of metal m , with the distribution

$$v_{\xi,t,m} = \left(\frac{v_{\xi,t,m}^{\text{UB}} - v_{\xi,t,m}^{\text{MED}}}{\Phi^{-1}(0.7)} \mathbb{I}(Z^{\text{COST}} \geq 0) + \frac{v_{\xi,t,m}^{\text{LB}} - v_{\xi,t,m}^{\text{MED}}}{\Phi^{-1}(0.3)} \mathbb{I}(Z^{\text{COST}} < 0) \right) Z^{\text{COST}} + v_{\xi,t,m}^{\text{MED}},$$

where Φ is the cumulative distribution function for the standard normal distribution. Here, the randomness is described by a single random variable Z^{COST} that is distributed as a truncated standard normal on $[\Phi^{-1}(0.3), \Phi^{-1}(0.7)]$. The marginal distributions for each $v_{\xi,t,m}$ are described by two truncated normal distributions, one for samples above the median and another for those below. The distributions are constructed so that $v_{\xi,t,m}^{\text{MED}}$ matches the median of $v_{\xi,t,m}$ and the HPD interval $[v_{\xi,t,m}^{\text{LB}}, v_{\xi,t,m}^{\text{UB}}]$ defines an equal-tailed 40% credible interval for $v_{\xi,t,m}$. We again generate a discrete distribution via two Gaussian quadratures for Z^{COST} , one on the interval $[\Phi^{-1}(0.3), 0]$ and one on $[0, \Phi^{-1}(0.7)]$, with $\lfloor \frac{n_c}{2} \rfloor$ samples allocated to each. The quadrature yields values $v_{(\xi,\zeta),t,m}$ and probabilities p_{ζ}^{COST} for each scenario $\zeta \in \llbracket n_c \rrbracket$.³ This approach only guarantees that the first $n_c - 2$ moments of the discrete distribution match the underlying distribution, but ensures that scenario observations across time lie at the same cumulative probability level of the underlying distributions. Although the observations of Z^{COST} from the Gaussian quadrature are identical in each stage, the distribution parameters $(v_{\xi,t,m}^{\text{MED}}, v_{\xi,t,m}^{\text{LB}}, v_{\xi,t,m}^{\text{UB}})$ are derived from the demand observation and therefore follow the same multistage structure as in the demand scenarios.

From the metal price observations, we construct scenario-dependent cost parameters. Consider some material cost parameter c (e.g., cost of lithium carbonate, cost of LFP cathode powder), where \bar{c} gives the deterministic value of this parameter from EverBatt. Let PC_m be the proportion by mass of the material composed of the metal m . We compute the base cost $c_{\xi}^{\text{BASE}} = \bar{c} - \sum_{m \in \mathcal{M}} PC_m v_{\xi,0,m}^{\text{MED}}$, which is the cost of the material excluding the value of the metals it contains. For cost index ζ , contributions from metal prices are added back to the base cost, $c_{(\xi,\zeta),t} = c_{\xi}^{\text{BASE}} + \sum_{m \in \mathcal{M}} PC_m v_{(\xi,\zeta),t,m}$. Then, the cost coefficients in (4a) are computed as the sum of the relevant scenario-dependent material cost time series $c_{(\xi,\zeta),t}$ and other utility cost terms. Figure 3 shows a set of cost scenarios generated with this method.

5.3 Multistage Scenario Tree

We now connect this method of scenario generation to the notation introduced in Section 3. The set of scenario tree nodes at stage σ is $\Omega_{\sigma} = \{\text{NCX, LFP}\} \times \llbracket n_d \rrbracket^{\sigma} \times \llbracket n_c \rrbracket$. The total number of scenarios (i.e., leaf nodes in the multistage tree) is $|\Omega_S| = 2n_d^S n_c$. For some stage $\sigma \in \mathcal{S}$ and node $\omega = (\psi, \xi, \zeta) \in \Omega_{\sigma}$, associated probabilities are given by $p_{\omega} = \frac{1}{2} p_{\zeta}^{\text{COST}} \prod_{\sigma'=1}^{\sigma} p_{\xi_{\sigma'},t}^{\text{EV}}$, demand and supply by $d_{\omega,z,t,i} = d_{(\psi,\xi),z,t,i}$ and $s_{\omega,z,t,i} = s_{(\psi,\xi),z,t,i}$, and material costs by $c_{\omega,t} = c_{(\xi,\zeta),t}$. The ancestor function for node $\omega \in \Omega_{\sigma}$ is defined as

$$a_{\omega}(t) = \begin{cases} (\psi, \xi_{1:\sigma_t}, \zeta) & \sigma_t \leq \sigma \\ (\psi, \xi, \zeta) & \text{otherwise,} \end{cases}$$

where $\xi_{1:\sigma_t}$ contains the first σ_t entries of ξ . If period t is associated with an earlier stage than node ω , the ancestor node is obtained by removing realizations of the demand randomness at stages after σ_t , while retaining the cost

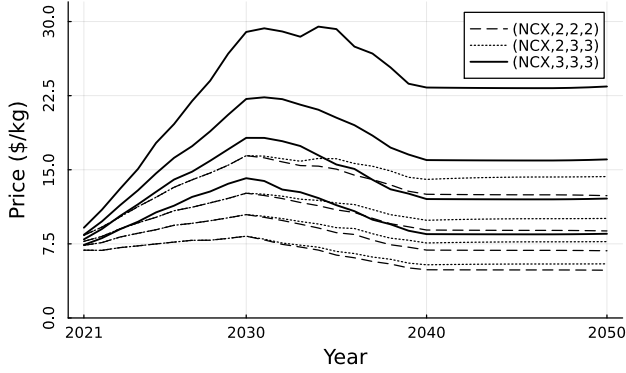


Figure 3: Four cost scenarios ($S = 3$, $n_c = n_d = 4$) for the value v of lithium carbonate under demand scenario $(\psi, \xi) = (\text{NCX}, 2, 2, 2)$ (low EV demand), demand scenario $(\text{NCX}, 3, 3, 3)$ (high demand), and demand scenario $(\text{NCX}, 2, 3, 3)$ (mixed demand).

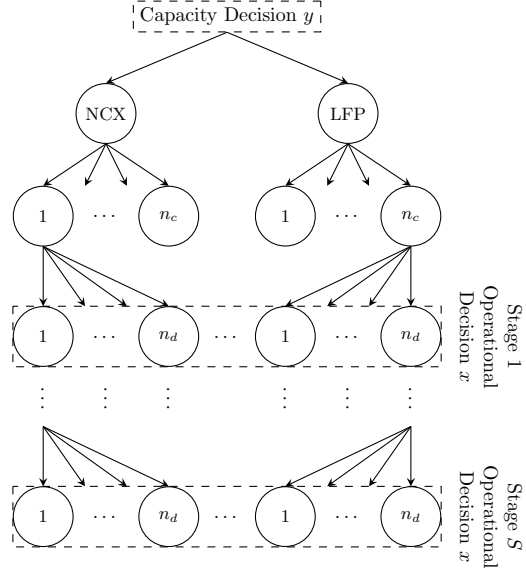


Figure 4: Multistage scenario tree and relative placement of capacity and operational decisions. Within each market share node (NCX, LFP), there are n_c cost nodes, and there are n_d new demand nodes for each node in the previous stage. Due to correlations between material cost and EV demand, cost parameters vary between demand nodes.

and market share realizations ζ and ψ . The multistage scenario tree and relative timing of decisions from models (P) and (PMI) are depicted in Figure 4.

Importantly, this scenario tree structure yields natural groupings for the decomposition discussed in Section 4.2. As ζ varies in the set $\llbracket n_c \rrbracket$, the scenario supply $s_{\omega, z, t, i}$ and demand $d_{\omega, z, t, i}$ do not change. Thus, a natural grouping at the first stage is $\mathcal{G}_{\psi, \xi} = \{(\psi, \xi, \zeta)\}_{\zeta=1}^{n_c}$ for $(\psi, \xi) \in \{\text{NCX}, \text{LFP}\} \times \llbracket n_d \rrbracket$, with $n_g = 2n_d$.

6 Computational Results and Case Studies

In this section, we computationally evaluate the effectiveness of the aPWL algorithm and decomposition schemes and discuss the insights obtained from the optimal solutions to our models. Numerical experiments are conducted in Julia 1.9 on dual 48-core AMD EPYC 9474F@3.60 GHz processors with 386 GB of RAM, allowing for parallelization over 96 cores. Linear and mixed-integer problems are solved with Gurobi 10.0. We use BARON 23.6.23 with CPLEX 22.1 and the embedded version of Ipopt as the mixed-integer and nonlinear subsolvers. Problems are solved to a relative optimality tolerance of 10^{-4} and a primal feasibility tolerance of 10^{-8} .

6.1 Concave Minimization Algorithms

We first evaluate the performance of aPWL (Algorithm 1) and the impact of the reformulated problem in a setting where subproblems are solved in the extensive form without stage decomposition. These models have a single operational scenario, where supply and demand are taken from the SDS and NCX projections, and material costs are kept constant at the EverBatt values. To encourage greater branching on capacity variables, the direct recycling capacity is fixed to 0, encouraging investment in cathode production facilities in the optimal solution. The model contains a single zone, the United States (U.S.).

	Problem (P)						Problem (PMI)			
		aPWL		sB&B		BARON		aPWL		BARON
$\beta_{\text{U.S.}}$	n_y	Time (s)	# Iter	Time (s)	# Iter	Time (s)	n_y	Time (s)	# Iter	Time (s)
0.1	3,765	167.4	2	2,421.6	2,132	724.3	96	2.7	2	7.0
0.15	5,635	616.0	3	1,130.1	369	1,803.1	96	5.3	2	6.7
0.2	7,508	561.9	2	2,519.4	445	3,779.5	96	9.3	2	10.0
0.25	9,377	1,295.4	3	4,866.2	471	11,209.6	96	14.0	1	16.7
0.3	11,250	1,008.6	2	3,438.0	123	14,298.7	96	20.1	1	22.8
0.35	13,119	2,162.4	2	—	—	24,437.8	96	30.9	1	34.3
0.4	14,994	2,622.0	2	17,185.0	263	—	96	40.2	1	43.1
0.45	16,861	4,722.1	2	—	—	—	96	50.4	1	51.9
0.5	18,735	5,481.8	2	13,483.6	99	—	96	62.6	1	65.8

Table 1: Algorithm and formulation comparison for the extensive form of (P) and (PMI). A — indicates that the model was not solved within 10 hours. n_y gives the number of capacity variables, which have concave cost functions.

For the continuous problem (P), we compare aPWL to a finitely convergent spatial branch and bound algorithm (sB&B, Shtetman and Sahinidis 1998) and to the global optimization package BARON (Sahinidis 1996). For the reformulation (PMI), we compare aPWL to BARON. In this setting, we do not evaluate sB&B due to the presence of integrality constraints. To solve over discontinuous objective functions with BARON, we reformulate (5) with binary variables:

$$y \leq uz, \quad f(y) = \sum_i q_i y^{r_i} + wz, \quad z \in \{0, 1\}.$$

Table 1 compares performance in the deterministic setting by algorithm and model across a variety of scales, generated by varying the proportion $\beta_{\text{U.S.}}$ of the global EV market that is modeled. For the original formulation (P), aPWL significantly outperforms all other methods, solving all problems within the time limit, and can terminate up to 14x faster than both sB&B and BARON. Moreover, aPWL exhibits more consistent performance than sB&B as the problem scale increases. The reformulation (PMI) allows for extreme reductions in solve times, allowing global optima to be found in minutes with either aPWL or BARON. For the reformulation, aPWL slightly outperforms BARON on all problems.

6.2 Decomposition Approaches

We next evaluate the performance of the Benders' decomposition when solving subproblems within aPWL. These experiments use instances of the reformulated problem (PMI) with multiple operational scenarios. We compare different nodal groupings against solving the subproblem in its extensive form, without decomposition. The nodal groupings considered are the standard single-cut ($\mathcal{G}_1 = \Omega_1$) and multi-cut ($\mathcal{G}_\omega = \{\omega\} \forall \omega \in \Omega_1$) aggregation strategies, as well as the intermediate grouping discussed in Section 5.3 ($\mathcal{G}_{\psi,\xi} = \{(\psi, \xi, \zeta)\}_{\zeta=1}^{n_c} \forall (\psi, \xi) \in \{\text{NCX, LFP}\} \times \llbracket n_d \rrbracket$). The problems have two zones: $\mathcal{Z} = \{\text{U.S., China}\}$. A set of test cases are generated by varying the model scale ($\beta_{\text{U.S.}}, \beta_{\text{China}}$) and the number of scenarios $|\Omega_S| = 2n_d^S n_c$, with $n_c = n_d$ and $S = 3$ for all problems. As optimal solutions in this setting have nonzero cathode production capacity, we no longer fix direct recycling capacity to 0.

Table 2 shows the computational results of the aPWL algorithm with the various decomposition approaches. Benders' decompositions outperform the extensive form in all test cases. Further, the grouped-cut aggregation strategy outperforms both single-cut and multi-cut implementations, solving up to 38% faster than the next fastest approach. The grouped-cut strategy effectively balances the tradeoff between increased subproblem size from adding many cuts in each iteration and information loss from aggregating cuts. With grouped-cut aggregation, the decomposition improves solve times by up to 275x over the extensive form. As the scale β increases, solve times

$(\beta_{\text{U.S.}}, \beta_{\text{China}})$	$ \Omega_S $	Extensive Form	Benders' Single-Cut		Benders' Grouped-Cut		Benders' Multi-Cut	
		Time (s)	Time (s)	# Iter	Time (s)	# Iter	Time (s)	# Iter
(0.05, 0.125)	162	456.9	59.8	250 (7)	24.5	63 (8)	30.9	52 (7)
	1,250	17,334.7	210.4	307 (8)	63.0	53 (6)	100.5	46 (4)
	20,000	—	1,532.5	249 (7)	810.6	52 (5)	930.8	37 (3)
(0.1, 0.25)	162	280.0	59.2	261 (4)	19.5	63 (7)	19.3	45 (3)
	1,250	2,694.4	155.5	229 (2)	56.6	53 (3)	68.8	36 (4)
	20,000	—	1,576.2	240 (5)	727.9	52 (4)	1,168.3	40 (5)
(0.15, 0.375)	162	356.7	44.3	203 (1)	14.2	55 (1)	21.2	49 (3)
	1,250	2,019.9	175.8	270 (7)	59.6	52 (5)	93.5	45 (6)
	20,000	—	1,500.9	240 (4)	717.7	47 (1)	851.3	35 (2)
(0.2, 0.5)	162	747.6	52.0	244 (4)	16.1	64 (2)	17.5	43 (3)
	1,250	2,592.7	170.1	260 (7)	57.1	48 (2)	61.7	36 (2)
	20,000	—	1,564.0	239 (3)	759.2	50 (4)	985.3	36 (4)

Table 2: Subproblem decomposition algorithm performance. # Iter counts the total Benders' iterations across all subproblems, with the number of iterations of Algorithm 1 given in parentheses. A — indicates that the model was not solved within 10 hours.

	Case 1 (U.S.)			Case 2 (U.S. + China)		
	R0	DR0	DR1	R0	DR0	DR1
Cost (billion \$)	1,732.1	1,365.5	1,351.5	6,062.3	4,706.5	4,687.4
Energy Consumption (EJ)	25.9	25.6	24.3	92.0	90.7	88.7
GHG Emissions (Mt)	1,647.9	1,614.2	1,535.3	5,987.0	5,910.6	5,790.0

Table 3: Comparison of optimal solutions in expected cost and environmental impact over model horizon. R0 indicates the solution with no recycling capacity, DR0 the solution where no direct recycling is allowed, and DR1 the solution where all recycling methods are allowed.

decrease. This occurs due to the use of relative optimality tolerances, with objective values increasing at larger scales. However, the size of the reformulated model does not grow accordingly.

6.3 Optimal Investment Strategies

We analyze the optimal solutions of two cases. The first (Case 1) has a single zone for the U.S., with $\beta_{\text{U.S.}} = 0.2$. The second (Case 2) has two zones, one for the U.S. and one for China, with $(\beta_{\text{U.S.}}, \beta_{\text{China}}) = (0.2, 0.5)$. Both cases have 20,000 operational scenarios ($S = 3$, $n_c = n_d = 10$). The 20% and 50% of global EV market shares correspond approximately to projections for market share in the U.S. and China, respectively, through 2030 (IEA 2023). As direct recycling is newer and less commercialized than other recycling processes, we analyze two variations of each case: one where direct recycling facilities can be constructed (labeled DR1) and one where the direct recycling capacity is fixed to 0 (labeled DR0).

In Section A.3 of the appendix, we discuss how cost parameters vary between the U.S. and China and provide a sensitivity analysis on these values. This analysis shows that the optimal objective value and recycling solution are not sensitive to these location-dependent cost parameters, but the cathode production solution exhibits sensitivity to the cost of equipment in China.

Comparison of Impact

To demonstrate the value of recycling, we compare to a solution where no recycling capacity is constructed (labeled R0) in objective cost, total energy consumption, and greenhouse gas (GHG) emissions. Energy consumption and GHG emissions are evaluated in expectation over the operational scenarios and aggregated over the model horizon.

These metrics are calculated by the EverBatt environmental impact model (Dai et al. 2019) and include the impact of recycling and cathode production processes as well as the upstream contribution of new materials that are purchased. Variation R0 provides baseline cost and environmental impact values for a solution in which new batteries are manufactured only using new materials. The improvement in these metrics relative to the R0 variation is due to the replacement of new materials with their recycled counterpart during new battery manufacturing and quantifies the impact of optimal investment in EV battery recycling capacity on the supply chain.

Table 3 compares the metrics in the variations R0, DR0, and DR1. Incorporating recycling into the supply chain reduces the total objective cost by about 22% in Case 2, variation DR0, with 0.3% additional reduction when direct recycling is allowed (variation DR1). In Case 1, the cost savings are more significant under direct recycling, increasing from 21% (DR0) to 22% (DR1). In both cases, energy consumption is marginally reduced ($\sim 1\%$) when non-direct recycling is adopted (DR0), with more significant reductions of 6% in Case 1 and 4% in Case 2 under direct recycling (DR1). Similarly, GHG emissions are reduced 1 – 2% by non-direct recycling (DR0), and up to 7% by direct recycling (DR1). Although there are large, comparable cost savings under direct or non-direct recycling, improvements in environmental impact are more significant under direct recycling, especially when only considering production in the U.S. This result can be partially attributed to the additional energy consumption and emissions from the cathode production step, which is needed when hydrometallurgical recycling is used but avoided with direct recycling.

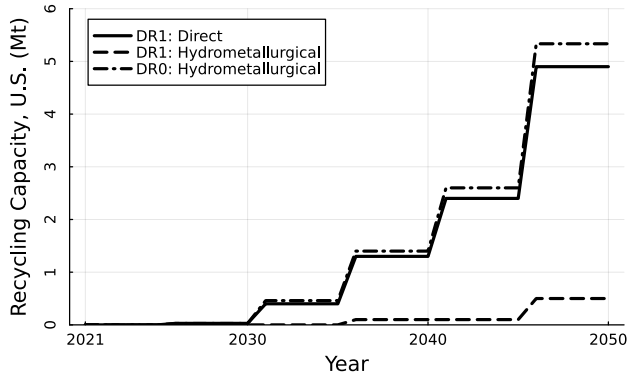
Optimal Investment Plan

Figure 5 depicts the optimal capacity decisions for the variations DR1 and DR0 of both cases. In Case 1, when direct recycling is allowed (variation DR1), the U.S. primarily constructs direct recycling capacity starting in 2026, supplemented by a smaller amount of hydrometallurgical capacity. The optimal solution constructs neither pyrometallurgical capacity nor cathode production capacity. When direct recycling cannot be constructed (variation DR0), the U.S. constructs a comparable amount of total recycling capacity, with direct recycling facilities replaced with hydrometallurgical. To produce cathode powder from recycled material, cathode production capacity for NMC(622) and NMC(811) is constructed in this variation. As of 2023, 650 kt of U.S. battery recycling capacity is announced to be completed by 2030 (Tankou and Hall 2023), which is greater than the optimal capacity of 400 kt recommended by our model in the DR1 variation and the 460 kt recommended in the DR0 variation. However, the announced capacity exceeds expectations for the available supply of retired batteries, suggesting potential overinvestment in recycling facilities (ABI Research 2024).

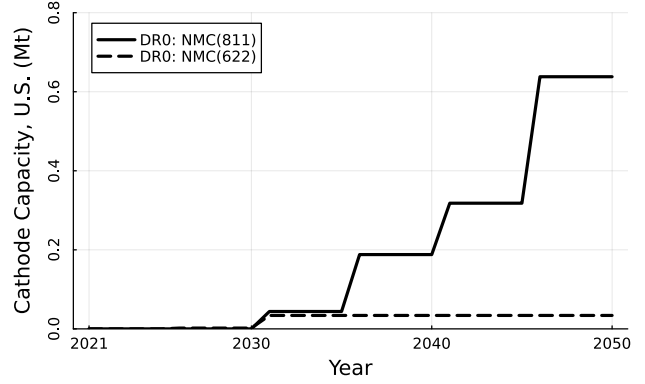
In the DR1 variation of Case 2, a mixture of hydrometallurgical and direct recycling capacity is constructed in China, starting in 2021. The U.S. constructs only direct recycling capacity in a lesser amount than in Case 1, starting in 2041. Cathode production capacity for all NMC chemistries is developed in China, and no cathode production capacity is installed in the U.S. At the operational scale, retired batteries are often transported from the U.S. to China to be recycled, then recycled cathode powder is transported back to the U.S. In the DR0 variation, only hydrometallurgical recycling capacity is constructed in China, and no recycling capacity is installed in the U.S. The total installed capacity is comparable to the total amount in the DR1 variation. Relative to the DR1 variation, NMC(811) and NMC(622) cathode production capacity is increased and capacity for NMC(532) and NMC(111) is eliminated.

Closed-Loop Recycled Material Usage

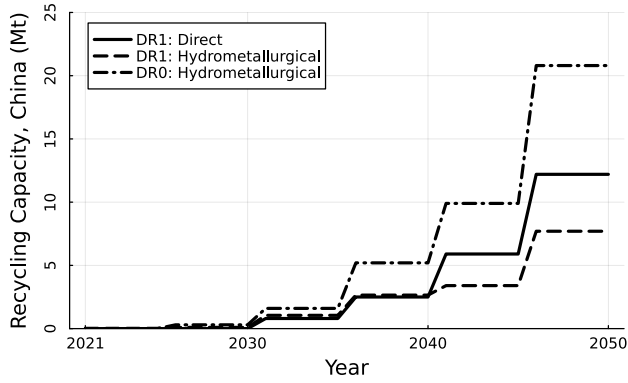
We consider the proportion of cathode material used to manufacture new batteries that is sourced from recycled batteries, which is called the closed-loop *recycling potential* for cathode material, defined by Xu et al. (2020). We



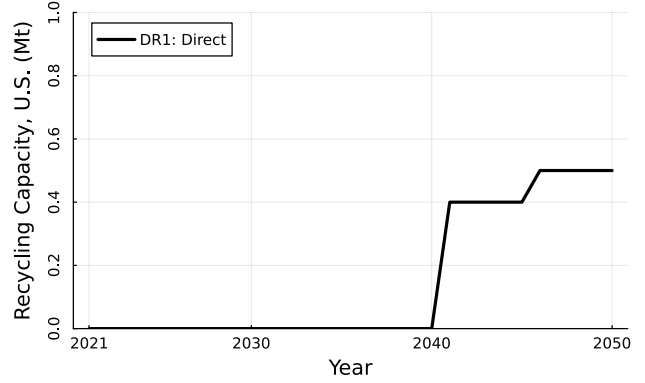
(a) Case 1, U.S. Recycling Capacity



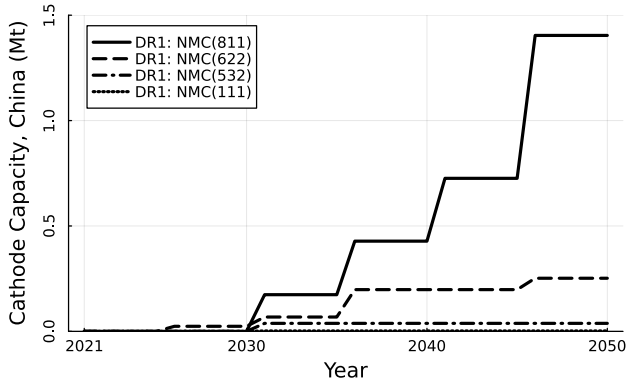
(b) Case 1, U.S. Cathode Production Capacity



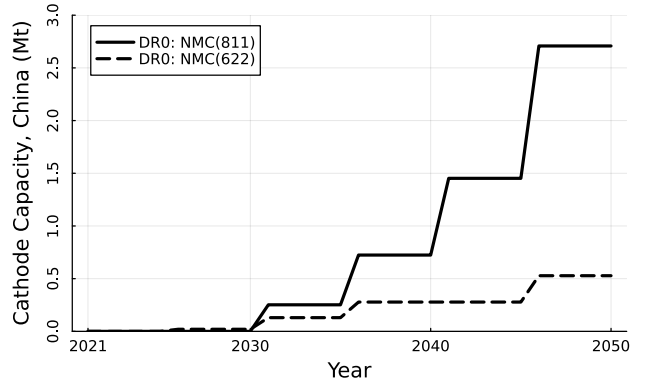
(c) Case 2, China Recycling Capacity



(d) Case 2, U.S. Recycling Capacity



(e) Case 2 DR1, China Cathode Production Capacity



(f) Case 2 DR0, China Cathode Production Capacity

Figure 5: Optimal capacity investment decisions for recycling and cathode production facilities by zone. No cathode production capacity is constructed for the DR1 variation of Case 1. Recycling capacity solutions for DR0 and DR1 models are shown on the same plots.

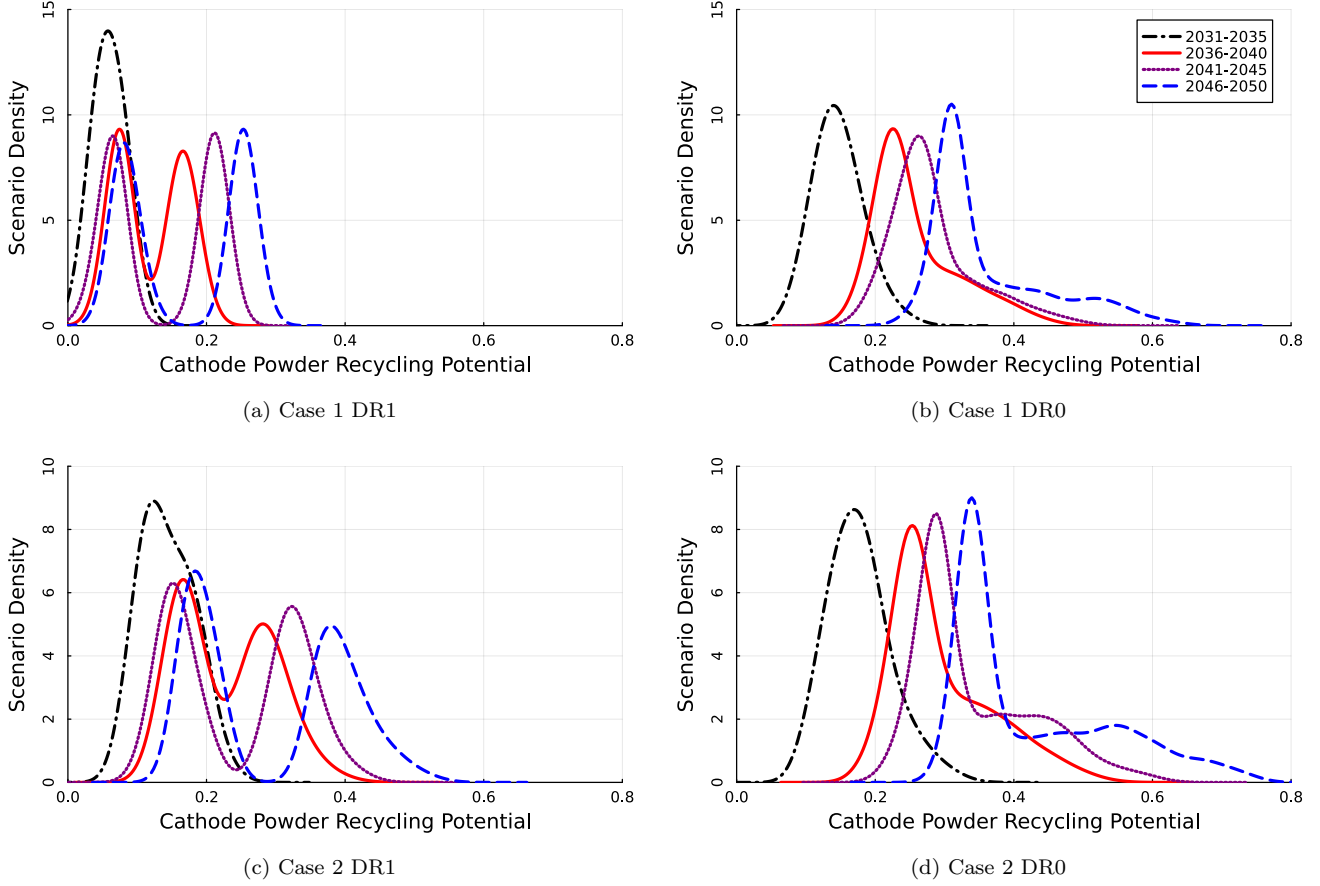


Figure 6: Kernel density estimation of the proportion of cathode powder used in new battery manufacturing that is produced via recycling (i.e., recycling potential of cathode powder) across operational scenarios, indexed by planning period.

compute the recycling potential for each scenario $\omega \in \Omega_S$ and planning period l as

$$\frac{\sum_{z \in \mathcal{Z}, k \in \mathcal{K}^{CP}, t \in \mathcal{T}_l} x_{z,a_\omega(t),t,k}^{\text{INV,NB}}}{\sum_{z \in \mathcal{Z}, k \in \mathcal{K}^{CP}, t \in \mathcal{T}_l} \left(x_{z,a_\omega(t),t,k}^{\text{INV,NB}} + x_{z,a_\omega(t),t,k}^{\text{NM,NB}} \right)}. \quad (12)$$

A recycling potential of 50% means that, within the planning period, half of the cathode material used in new battery manufacturing comes from recycled sources.

Figures 6 and 7 visualize the recycling potential as a distribution over the operational scenarios. Figure 6 shows the density of the recycling potential (i.e., a smoothed probability density function), and Figure 7 gives an empirical cumulative distribution function. We observe that scenarios with higher prominence of LFP cathode powders have lower recycling potential than NCX scenarios. Because LFP powders do not contain cobalt, they are inexpensive to manufacture from new materials. This property reduces the cost effectiveness of recycling and gives the distributions a bimodal structure, where the first mode corresponds to LFP scenarios and the second to NCX scenarios.

Furthermore, solutions that construct hydrometallurgical recycling capacity (i.e., Case 1 DR0 and both Case 2 variations) yield right-tailed distributions. Recall that hydrometallurgical recycling recovers cathode precursors, while direct recycling recovers cathode powder. Recycled precursors can be manufactured into any cathode powder chemistry, allowing these materials to be used in manufacturing even as battery demand shifts between chemistries.

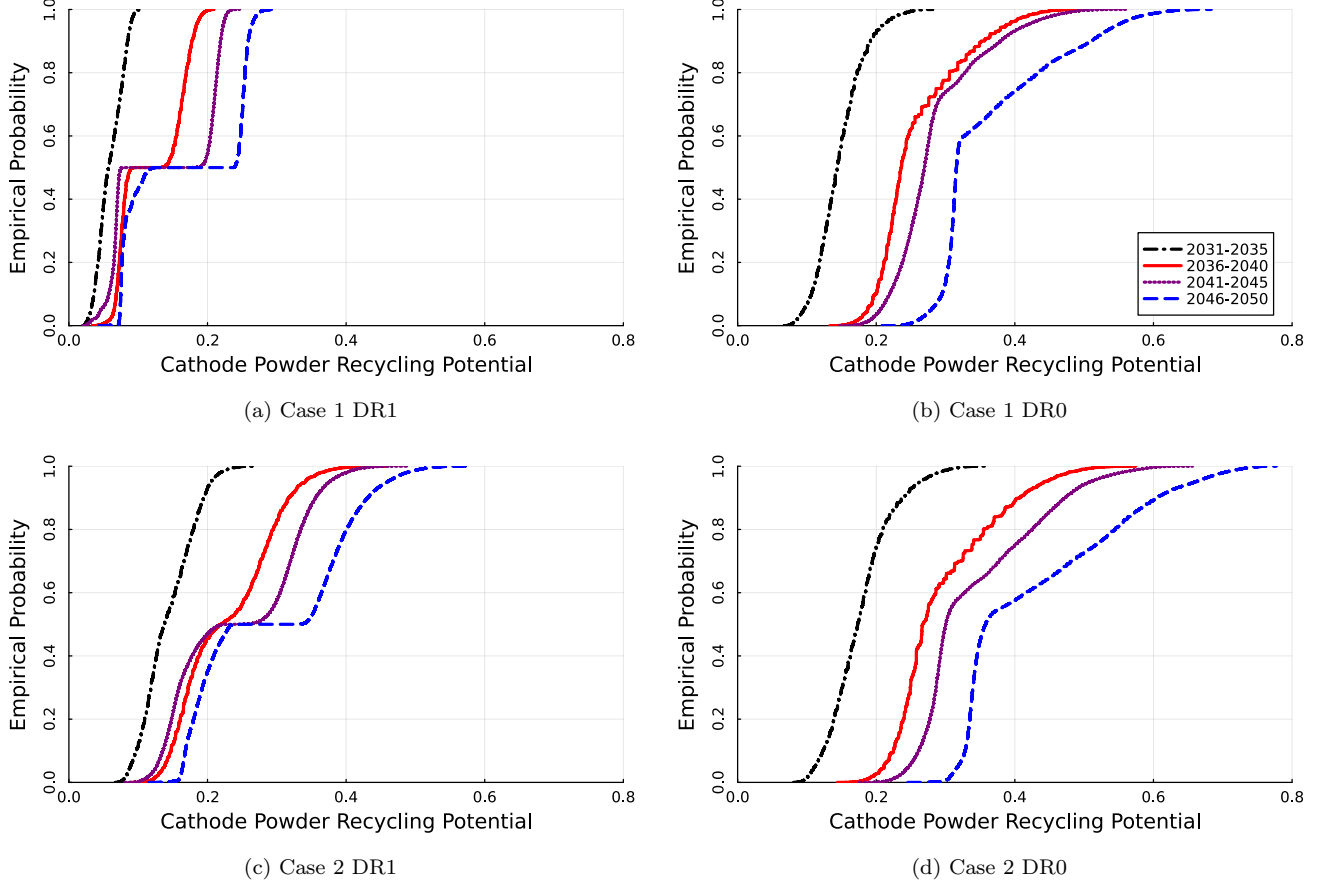


Figure 7: Empirical cumulative density function of the proportion of cathode powder used in new battery manufacturing that is produced via recycling (i.e., recycling potential of cathode powder) across operational scenarios, indexed by planning period.

Alternatively, cathode powder recovered from direct recycling can only be used to manufacture batteries of the same chemistry. Especially in DR0 solutions, the prevalence of hydrometallurgical recycling allows flexibility in how recycled materials are used in new battery manufacturing and allows for high rates of recycled material usage in some scenarios. This result emphasizes a hidden benefit of hydrometallurgical recycling over direct methods when considering variable cathode chemistry demand, even though minimum-cost solutions prefer direct recycling.

Due to the low manufacturing cost of LFP powder, in the DR1 variations, the mode corresponding to LFP scenarios does not shift towards higher recycling potential as additional capacity becomes available in later planning periods. In DR0 variations, the flexibility of hydrometallurgical recycling allows lithium recovered from LFP batteries to be used to manufacture cathode powders of other, more expensive chemistries. This increases the recycling potential of the first mode in these variations, even though the expensive chemistries are less prevalent in LFP scenarios.

In the DR1 variations, the maximum level of recycling potential across scenarios approaches 30% in Case 1 and 60% in Case 2, and the expected recycling potential is 12% in Case 1 and 23% in Case 2. Due to the increased investment in hydrometallurgical capacity in DR0 variations, the maximum recycling potential increases to 70% in Case 1 and 80% in Case 2, and the expected potential increases to 27% in Case 1 and 32% in Case 2.

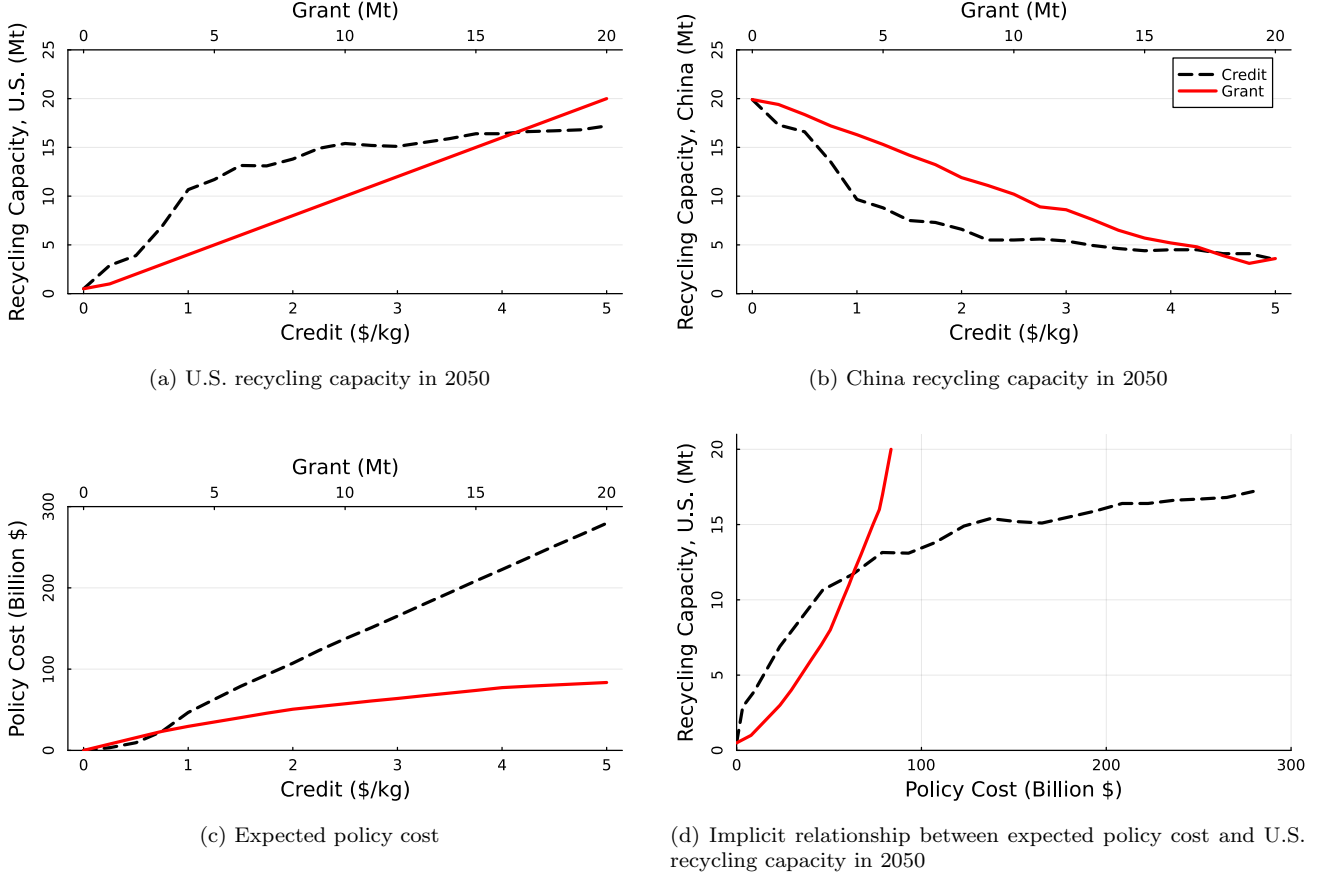


Figure 8: Impact of grant and credit policy level on installed recycling capacity in 2050 (a,b) and expected policy cost (c). (d) shows implicitly how expenditure on each policy impacts installed U.S. recycling capacity in 2050.

6.4 Policy Analysis: Capacity Grants or Production Credits?

We consider the impact of two fundamental policy instruments on the supply chain: *capacity grants* for the installation of recycling capacity and *production credits* paid for recycling throughput. We provide insights on which instrument more effectively shapes U.S. domestic recycling capability.

The U.S. Department of Energy has provided grants for recycling facilities, including \$6 billion of grants announced in 2022 (U.S. Department of Energy 2025a,b), and the Inflation Reduction Act of 2022 established credits for the domestic manufacture of critical minerals and battery components, which includes domestic recycling of EV batteries (Mehdi and Moerenhout 2023, Internal Revenue Service 2025). We study the implementation of these policies in the U.S. under Case 2, with zones for the U.S. and China. Capacity grants are modeled as a lower bound p^{GRANT} on installed recycling capacity in the U.S. by 2031, i.e., the start of the third planning period. That is, we enforce in model (PMI) the following constraint:

$$\sum_{j \in \mathcal{J}} u^{\text{REC}} y_{\text{U.S.},3,j}^{\text{REC}} + y_{\text{U.S.},3,j,+}^{\text{REC}} \geq p^{\text{GRANT}}. \quad (13)$$

Costs associated with the minimum capacity p^{GRANT} are covered by the grant and are ignored by the recycler. Additional capacity construction incurs additional cost. Credits are modeled by adding a credit revenue term to

Capacity Grant (Mt)	—	5.0	10.0	20.0	—	—	—
Recycling Credit (\$/kg)	—	—	—	—	1	3	5
U.S. Recycling, 2050 (Mt)	0.5	5.0	10.0	20.0	10.7	15.1	17.2
China Recycling, 2050 (Mt)	19.9	15.3	10.2	3.6	9.7	5.4	3.5
U.S. Recycling Potential	1.5%	11.6%	15.0%	20.0%	23.9%	24.3%	24.7%
China Recycling Potential	26.6%	23.1%	21.3%	19.0%	14.3%	13.2%	12.3%
Aggregate Recycling Potential	22.7%	22.8%	22.4%	22.0%	21.5%	21.9%	21.3%
Policy Cost (billion \$)	—	34.9	57.4	83.6	46.7	165.2	279.5

Table 4: Impact of grants and credits on recycling metrics under the optimal solution in Case 2. Metrics include installed recycling capacity in 2050, expected recycling potential (12), and the expected policy cost.

the objective:

$$-p^{\text{CRED}} \sum_{t \in \mathcal{T}} \sum_{\omega \in \Omega_{\sigma_t}} \sum_{j \in \mathcal{J}, i \in \mathcal{I}} (1 - \gamma)^{t-1} p_{\omega} x_{\omega, \text{U.S.}, t, i, j}^{\text{RB, RM}},$$

where p^{CRED} gives the recycling credit value per unit mass of throughput. For reference, the expected undiscounted recycling cost (including planning and operational costs) per unit mass of throughput in Case 2 is \$1.69/kg.

We consider several metrics to measure the impact of the policies:

1. the installed capacity in each zone in 2050;
2. the *policy cost*: annual planning costs incurred by the grant capacity after 2031 and expected credit costs; and
3. the expected recycling potential for cathode powder (12), in aggregate and for materials handled exclusively within a zone.

Figure 8 shows how the installed capacity and policy cost vary with different levels of the grant p^{GRANT} and credit p^{CRED} , and Figure 8d shows the implicit relationship between the policy cost at different levels of each policy and the amount of installed capacity in the U.S. in 2050. That is, Figure 8d demonstrates how much domestic recycling capacity results from a given amount of expenditure on each policy. For a few select levels of each policy, Table 4 compares the corresponding value for each metric against a baseline solution without intervention.

Figures 8a and 8b show that, in most cases, both grants and credits shift installed recycling capacity from China to the U.S. without drastically changing the total amount of constructed capacity. However, for a large capacity grants (e.g., $p^{\text{GRANT}} = 20$ Mt), the total recycling capacity may increase sizably, by up to 15%. The capacity lower bound (13) for grants is typically binding, meaning that U.S. capacity grows linearly as a function of the grant capacity. Alternatively, credits exhibit sublinear growth, so, for large credits, increasing the credit amount does not drastically increase the U.S. recycling capacity. In Figure 8c we observe that the marginal policy cost of grant capacity is decreasing, suggesting that less expensive recycling capacity is installed to meet the capacity requirement from large grants. The expected cost of credits grows superlinearly at low ($< \$1/\text{kg}$) credit levels, then increases linearly. Figure 8d shows that, at the same expected cost, credits encourage greater investment in U.S. recycling capacity than grants when the expected policy cost is low ($< \$65$ billion). At higher expected policy costs, grants are more cost-effective for developing U.S. capacity.

Table 4 shows how operational recycling decisions respond to the policies. We find that both policies encourage the use of domestically recycled materials for manufacturing within the U.S. by increasing the recycling potential in the U.S. and causing a corresponding decrease in China. Credit-based policies encourage higher rates of recycling in the U.S. than grant-based policies. However, credits slightly decrease the aggregate recycling potential compared to grants and the baseline, likely because they encourage recycling even at times when recycled materials cannot be used effectively in new battery manufacturing.

7 Conclusion

In this work, we propose a multistage stochastic optimization model for the design and operation of closed-loop EV battery recycling supply chains. We transform EverBatt, an evaluative framework for battery recycling cost and environmental impact, into a detailed, high-fidelity decision-making model that determines optimal recycling and cathode production investment strategies. We construct a procedure for generating multistage scenarios for new battery demand, retired battery supply, and material costs, leveraging state-of-the-art econometric models for critical mineral prices and EV demand. To solve our model, we introduce an algorithm for separable concave minimization over polyhedra that improves performance over existing algorithms and a cut grouping strategy for Benders' decomposition that converges faster than standard approaches. We find an equivalent formulation of our model which reduces solve times by introducing integrality constraints. Analysis of the optimal solutions shows large improvements in the cost of manufacturing new batteries when recycling is incorporated into the supply chain, as well as reductions in the environmental impact of battery manufacturing. We provide insights into the impact of recycling capacity grants and production credits on domestic investment in battery recycling, revealing that production credits encourage greater investment at lower policy costs, whereas grants become more cost-effective with higher policy expenditure. Overall, this methodology provides a comprehensive and flexible quantitative framework for recyclers, battery manufacturers, and policy makers to plan for the integration of recycling technologies into the supply chain.

Endnotes

1. Pourmohammadi et al. (2008) estimate η as 60% for recycled aluminum. Recycled carbon black is similarly discounted by $\eta \in [70\%, 85\%]$ relative to its virgin counterpart (Contec 2023).
2. Boer et al. (2024) do not provide projections for manganese prices. However, we find that manganese and copper prices are highly correlated. Price data from IMF (2022) between 2013 and 2021 show that manganese and copper prices have a correlation coefficient of 0.91. As validation, a correlation of prices between 1950 and 2010 from U.S. Geological Survey (2013) yields a coefficient of 0.85. Given this high correlation, we predict the median value and HPD bounds for manganese from the corresponding values for copper using a linear regression fitted on data from IMF (2022).
3. The quadrature probabilities are reweighted by $\frac{1}{2}$ to account for $\mathbb{P}(Z^{\text{COST}} \geq 0)$ and $\mathbb{P}(Z^{\text{COST}} < 0)$.

References

- ABI Research (2024) U.S. EV battery recycling industry faces challenge as input supply reaches only a quarter of capacity by 2030. Accessed December 2024, <https://www.abiresearch.com/press/us-ev-battery-recycling-industry-faces-challenge-as-input-supply-reaches-only-a-quarter-of-capacity-by-2030>.
- Adulyasak Y, Cordeau JF, Jans R (2015) Benders decomposition for production routing under demand uncertainty. *Operations Research* 63(4):851–867.
- Antolín-Díaz J, Petrella I, Rubio-Ramírez JF (2021) Structural scenario analysis with SVARs. *Journal of Monetary Economics* 117:798–815.
- Azzi A, Battini D, Faccio M, Persona A, Sgarbossa F (2014) Inventory holding costs measurement: a multi-case study. *The International Journal of Logistics Management* 25(1):109–132.
- BASF (2023) Partnership between BASF and Nanotech Energy will enable production of lithium-ion batteries in North America with locally recycled content and low CO2 footprint. Accessed June 2024, <https://www.basf.com/global/en/media/news-releases/2023/09/p-23-292.html>.

- Bazaraa MS, Sherali HD (1982) On the use of exact and heuristic cutting plane methods for the quadratic assignment problem. *Journal of the Operational Research Society* 33(11):991–1003.
- Benders JF (1962) Partitioning procedures for solving mixed-variables programming problems. *Numerische Mathematik* 4(1):238–252.
- Benson HP (1985) A finite algorithm for concave minimization over a polyhedron. *Naval Research Logistics Quarterly* 32(1):165–177.
- Birge JR, Louveaux F (2011) *Introduction to Stochastic Programming* (Springer Science & Business Media).
- Boer L, Pescatori A, Stuermer M (2024) Energy transition metals: bottleneck for net-zero emissions? *Journal of the European Economic Association* 22(1):200–229.
- Campagnol N, Pfeiffer A, Tryggstad C (2022) Capturing the battery value-chain opportunity. Accessed October 2023, <https://www.mckinsey.com/industries/electric-power-and-natural-gas/our-insights/capturing-the-battery-value-chain-opportunity>.
- Contec (2023) On the rise: the price of carbon black isn’t sustainable. Accessed December 2023, <https://contec.tech/price-of-carbon-black-sustainability>.
- Council of the European Union (2023) Council adopts new regulation on batteries and waste batteries. Accessed October 2023, <https://www.consilium.europa.eu/en/press/press-releases/2023/07/10/council-adopts-new-regulation-on-batteries-and-waste-batteries>.
- Dai Q, Spangenberg J, Ahmed S, Gaines L, Kelly JC, Wang M (2019) EverBatt: a closed-loop battery recycling cost and environmental impacts model. Technical report, Argonne National Lab.
- D’Ambrosio C, Lee J, Wächter A (2009) A global-optimization algorithm for mixed-integer nonlinear programs having separable non-convexity. *European Symposium on Algorithms*, 107–118.
- Falk JE, Soland RM (1969) An algorithm for separable nonconvex programming problems. *Management Science* 15(9):550–569.
- Feldman E, Lehrer FA, Ray TL (1966) Warehouse location under continuous economies of scale. *Management Science* 12(9):670–684.
- Harper G, Sommerville R, Kendrick E, Driscoll L, Slater P, Stolkin R, Walton A, Christensen P, Heidrich O, Lambert S, Abbott A, Ryder K, Gaines L, Anderson P (2019) Recycling lithium-ion batteries from electric vehicles. *Nature* 575:75–86.
- Horst R, Pardalos PM, Van Thoai N (2000) *Introduction to Global Optimization* (Springer Science & Business Media).
- Hoyer C, Kieckhäfer K, Spengler TS (2015) Technology and capacity planning for the recycling of lithium-ion electric vehicle batteries in Germany. *Journal of Business Economics* 85:505–544.
- IEA (2020) Global EV outlook 2020. Technical report, IEA.
- IEA (2022) Global supply chains of EV batteries. Technical report, IEA.
- IEA (2023) Global EV data explorer. Accessed August 2023, <https://www.iea.org/data-and-statistics/data-tools/global-ev-data-explorer>.
- IMF (2022) Primary commodity price system. Accessed December 2022, <https://data.imf.org/commodityprices>.
- Internal Revenue Service (2025) Advanced manufacturing production credit. Accessed June 2025, <https://www.irs.gov/credits-deductions/advanced-manufacturing-production-credit>.
- Kang DHP, Chen M, Ogunseitan OA (2013) Potential environmental and human health impacts of rechargeable lithium batteries in electronic waste. *Environmental Science & Technology* 47(10):5495–5503.
- Kneifel J, Webb D (2020) Life cycle costing manual for the Federal Energy Management Program. <https://doi.org/10.6028/NIST.HB.135-2020>.
- Lee SB, Luss H (1987) Multifacility-type capacity expansion planning: algorithms and complexities. *Operations Research* 35(2):249–253.
- Li L, Dababneh F, Zhao J (2018) Cost-effective supply chain for electric vehicle battery remanufacturing. *Applied Energy* 226:277–286.
- Li P, Huai Z, Jiang J (2023) Optimization of closed-loop supply chain network design under uncertainty: considering electric vehicle battery recycling. *Industrial Engineering and Applications*, volume 35 of *Advances in Transdisciplinary Engineering*, 182–190.

- Li S, Tirupati D (1994) Dynamic capacity expansion problem with multiple products: technology selection and timing of capacity additions. *Operations Research* 42(5):958–976.
- Magnanti TL, Stratila D (2004) Separable concave optimization approximately equals piecewise linear optimization. *Integer Programming and Combinatorial Optimization*, 234–243.
- Makuza B, Tian Q, Guo X, Chattopadhyay K, Yu D (2021) Pyrometallurgical options for recycling spent lithium-ion batteries: a comprehensive review. *Journal of Power Sources* 491:229622.
- Marano V, Onori S, Guezennec Y, Rizzoni G, Madella N (2009) Lithium-ion batteries life estimation for plug-in hybrid electric vehicles. *2009 IEEE Vehicle Power and Propulsion Conference*, 536–543.
- Martínez-Costa C, Mas-Machuca M, Benedito E, Corominas A (2014) A review of mathematical programming models for strategic capacity planning in manufacturing. *International Journal of Production Economics* 153:66–85.
- Mehdi A, Moerenhout T (2023) The IRA and the US battery supply chain: one year on. Accessed June 2025, <https://www.energypolicy.columbia.edu/publications/the-ira-and-the-us-battery-supply-chain-one-year-on>.
- Miller III AC, Rice TR (1983) Discrete approximations of probability distributions. *Management Science* 29(3):352–362.
- Ohnsman A (2022) VW and Audi to recycle EV batteries through Tesla cofounder’s company. Accessed June 2024, <https://www.forbes.com/sites/alanohnsman/2022/07/12/vw-and-audi-to-recycle-ev-batteries-through-tesla-cofounders-company>.
- Pardalos PM, Romeijn HE (2002) *Handbook of Global Optimization*, volume 2 (Springer).
- Pardalos PM, Rosen JB (1986) Methods for global concave minimization: a bibliographic survey. *SIAM Review* 28(3):367–379.
- Pourmohammadi H, Rahimi M, Dessouky M (2008) Sustainable reverse logistics for distribution of industrial waste/byproducts: a joint optimization of operation and environmental costs. *Supply Chain Forum: An International Journal*, volume 9, 2–17.
- Raghavachari M (1969) On connections between zero-one integer programming and concave programming under linear constraints. *Operations Research* 17(4):680–684.
- Rajagopalan S, Singh MR, Morton TE (1998) Capacity expansion and replacement in growing markets with uncertain technological breakthroughs. *Management Science* 44(1):12–30.
- Rosen JB (1983) Global minimization of a linearly constrained concave function by partition of feasible domain. *Mathematics of Operations Research* 8(2):215–230.
- Rosenberg S, Glöser-Chahoud S, Huster S, Schultmann F (2023) A dynamic network design model with capacity expansions for EoL traction battery recycling – a case study of an OEM in Germany. *Waste Management* 160:12–22.
- Sahinidis NV (1996) BARON: a general purpose global optimization software package. *Journal of Global Optimization* 8:201–205.
- Shectman JP, Sahinidis NV (1998) A finite algorithm for global minimization of separable concave programs. *Journal of Global Optimization* 12:1–36.
- Tadaros M, Migdalas A, Samuelsson B, Segerstedt A (2022) Location of facilities and network design for reverse logistics of lithium-ion batteries in Sweden. *Operational Research* 22:895–915.
- Tankou A, Hall D (2023) Will the U.S. EV battery recycling industry be ready for millions of end-of-life batteries? Accessed December 2024, <https://theicct.org/us-ev-battery-recycling-end-of-life-batteries-sept23>.
- Tuy H (1964) Concave programming with linear constraints. *Doklady Akademii Nauk* 159(1):32–35.
- US Department of Energy (2025a) Battery manufacturing and recycling grants. Accessed May 2025, <https://www.energy.gov/mesc/battery-manufacturing-and-recycling-grants>.
- US Department of Energy (2025b) Battery materials processing grants. Accessed May 2025, <https://www.energy.gov/mesc/battery-materials-processing-grants>.
- US Geological Survey (2013) Metal prices in the United States through 2010. Technical report, U.S. Geological Survey, <http://dx.doi.org/10.3133/sir20125188>.
- US Geological Survey (2022) 2022 final list of critical minerals. Accessed October 2023, <https://www.usgs.gov/news/national-news-release/us-geological-survey-releases-2022-list-critical-minerals>.
- Van Mieghem JA (2003) Capacity management, investment, and hedging: review and recent developments. *Manufacturing & Service Operations Management* 5(4):269–302.

- Van Slyke RM, Wets R (1969) L-shaped linear programs with applications to optimal control and stochastic programming. *SIAM Journal on Applied Mathematics* 17(4):638–663.
- Wang L, Wang X, Yang W (2020) Optimal design of electric vehicle battery recycling network – from the perspective of electric vehicle manufacturers. *Applied Energy* 275:115328.
- Wu J, Zheng M, Liu T, Wang Y, Liu Y, Nai J, Zhang L, Zhang S, Tao X (2023) Direct recovery: a sustainable recycling technology for spent lithium-ion battery. *Energy Storage Materials* 54:120–134.
- Xu C, Dai Q, Gaines L, Hu M, Tukker A, Steubing B (2020) Future material demand for automotive lithium-based batteries. *Communications Materials* 1:99.
- Yao Y, Zhu M, Zhao Z, Tong B, Fan Y, Hua Z (2018) Hydrometallurgical processes for recycling spent lithium-ion batteries: a critical review. *ACS Sustainable Chemistry & Engineering* 6(11):13611–13627.

A Appendix

This appendix is organized as follows. Section A.1 contains tables that summarize the data and variables used in our models. Section A.2 describes the computation of the average battery mass parameter used in demand scenario generation. Section A.3 describes how cost parameters vary across zones and conducts a sensitivity analysis on these parameters. Section A.4 provides proofs of our results.

A.1 Summary of Model Data

Tables A.1, A.2, and A.3 give descriptions of the index sets, constant parameters, and variables used to define the models (P) and (PMI).

Table A.1: Sets

\mathcal{I}	Set of battery chemistries
\mathcal{J}	Set of recycling processes
\mathcal{K}	Set of materials encountered during recycling and manufacturing
\mathcal{K}^{CP}	Set of cathode powders
\mathcal{L}	Set of planning periods in the model horizon
$\mathcal{N}_{l,k}^{\text{CP}}$	Set of cathode production line indices used to produce material $k \in \mathcal{K}^{\text{CP}}$ during planning period $l \in \mathcal{L}$
$\mathcal{N}_l^{\text{REC}}$	Set of recycling facility indices during planning period $l \in \mathcal{L}$
\mathcal{S}	Set of stages in the multistage scenario tree
\mathcal{T}	Set of time periods in the model horizon
\mathcal{T}_l	Set of time periods associated with planning period $l \in \mathcal{L}$
\mathcal{Z}	Set of zones in which production facilities can be located
Ω_σ	Set of multistage scenario tree nodes at stage $\sigma \in \mathcal{S}$

Table A.2: Parameters

$a_\omega(t)$	Ancestor node of node $\omega \in \cup_{\sigma \in \mathcal{S}} \Omega_\sigma$ at period $t \in \mathcal{T}$
$c_{\omega,z,t,k}^{\text{CP}}$	Variable cost of producing one unit of material $k \in \mathcal{K}^{\text{CP}}$ via cathode production in time period $t \in \mathcal{T}$, zone $z \in \mathcal{Z}$ and node $\omega \in \Omega_{\sigma_t}$
$c_{\omega,t,k}^{\text{CP,NM}}$	Cost per unit of material $k \in \mathcal{K} \setminus \mathcal{K}^{\text{CP}}$ purchased new to manufacture cathode powder in time period $t \in \mathcal{T}$ and node $\omega \in \Omega_{\sigma_t}$
$c_{\omega,z,t,k}^{\text{MC}}$	Variable cost for generating one unit of material $k \in \mathcal{K} \setminus \mathcal{K}^{\text{CP}}$ via material conversion in time period $t \in \mathcal{T}$, zone $z \in \mathcal{Z}$ and node $\omega \in \Omega_{\sigma_t}$
$c_{\omega,t,k}^{\text{NB,NM}}$	Cost per unit of material $k \in \mathcal{K}$ purchased new to manufacture batteries in time period $t \in \mathcal{T}$ and node $\omega \in \Omega_{\sigma_t}$
$c_{\omega,z,t,i,j}^{\text{REC}}$	Variable cost per unit mass of battery of chemistry $i \in \mathcal{I}$ recycled with process $j \in \mathcal{J}$ in time period $t \in \mathcal{T}$, zone $z \in \mathcal{Z}$ and node $\omega \in \Omega_{\sigma_t}$
$c_{z,z'}^{\text{TR,RB}}$	Cost per unit mass of battery transported from zone $z \in \mathcal{Z}$ to zone $z' \in \mathcal{Z} \setminus \{z\}$
$c_{z,z'}^{\text{TR,RM}}$	Cost to transport a unit of recycled material from zone $z \in \mathcal{Z}$ to zone $z' \in \mathcal{Z} \setminus \{z\}$
$C_{\omega,t}^{\text{OP}}$	Operational costs as a function of operational decisions in time period $t \in \mathcal{T}$ and node $\omega \in \Omega_{\sigma_t}$
C_t^{PL}	Planning costs as a function of capacity decisions in time period $t \in \mathcal{T}$
$\overline{C}_t^{\text{PL}}$	Planning costs as a function of capacity decisions in time period $t \in \mathcal{T}$ for the reformulated capacity variable structure

$d_{\omega,z,t,i}$	Demand for batteries of chemistry $i \in \mathcal{I}$ in time period $t \in \mathcal{T}$, zone $z \in \mathcal{Z}$ and node $\omega \in \Omega_{\sigma_t}$
$f_{z,k}^{\text{CP}}$	Concave function mapping cathode production capacity for a line producing material $k \in \mathcal{K}^{\text{CP}}$ in zone $z \in \mathcal{Z}$ to annual labor and capital cost
$f_{z,j}^{\text{REC}}$	Concave function mapping recycling capacity for process $j \in \mathcal{J}$ in zone $z \in \mathcal{Z}$ to annual labor and capital cost
l_t	Planning period associated with time period $t \in \mathcal{T}$
p_ω	Probability associated with node $\omega \in \cup_{\sigma \in \mathcal{S}} \Omega_\sigma$
$s_{\omega,z,t,i}$	Supply of batteries of chemistry $i \in \mathcal{I}$ in time period $t \in \mathcal{T}$, zone $z \in \mathcal{Z}$ and node $\omega \in \Omega_{\sigma_t}$
u^{CP}	Maximum capacity of a cathode production line
u^{REC}	Maximum capacity of a recycling process at each facility
$v_{\omega,t,k}$	Value per unit of material $k \in \mathcal{K}$ in time period $t \in \mathcal{T}$ and node $\omega \in \Omega_{\sigma_t}$
$\Delta_{k',k}^{\text{CP}}$	Amount of material $k \in \mathcal{K} \setminus \mathcal{K}^{\text{CP}}$ used to produce one unit of material $k' \in \mathcal{K}^{\text{CP}}$ via cathode production
$\Delta_{k',k}^{\text{MC}}$	Amount of material $k \in \mathcal{K} \setminus \mathcal{K}^{\text{CP}}$ used to produce one unit of material $k' \in \mathcal{K} \setminus \mathcal{K}^{\text{CP}}$ via material conversion
$\Delta_{i,k}^{\text{NB}}$	Amount of material $k \in \mathcal{K}$ used to produce a unit mass of battery of chemistry $i \in \mathcal{I}$
$\Delta_{k,i,j}^{\text{REC}}$	Amount of material $k \in \mathcal{K}$ generated by recycling a unit mass of battery of chemistry $i \in \mathcal{I}$ with process $j \in \mathcal{J}$
γ	Annual discount factor
η	Proportion of material value recovered when selling recycled material to the market
ρ	Proportion of material value incurred as annual inventory cost
σ_t	Stage associated with time period $t \in \mathcal{T} \cup \{0\}$

Table A.3: Variables

$x_{\omega,z,t,k}^{\text{CP,INV}}$	Amount of output material $k \in \mathcal{K}^{\text{CP}}$ from cathode production put in inventory in time period $t \in \mathcal{T}$, zone $z \in \mathcal{Z}$ and node $\omega \in \Omega_{\sigma_t}$
$x_{\omega,z,t,k}^{\text{INV}}$	Amount of recycled material $k \in \mathcal{K}$ in inventory in time period $t \in \mathcal{T}$, zone $z \in \mathcal{Z}$ and node $\omega \in \Omega_{\sigma_t}$
$x_{\omega,z,t,k}^{\text{INV,MC}}$	Amount of recycled material $k \in \mathcal{K} \setminus \mathcal{K}^{\text{CP}}$ used in material conversion in time period $t \in \mathcal{T}$, zone $z \in \mathcal{Z}$ and node $\omega \in \Omega_{\sigma_t}$
$x_{\omega,z,t,k}^{\text{INV,NB}}$	Amount of recycled material $k \in \mathcal{K}^{\text{CP}}$ used to produce new batteries in time period $t \in \mathcal{T}$, zone $z \in \mathcal{Z}$ and node $\omega \in \Omega_{\sigma_t}$
$x_{\omega,z,t,k}^{\text{MC,CP}}$	Amount of output material $k \in \mathcal{K} \setminus \mathcal{K}^{\text{CP}}$ from material conversion used for cathode production in time period $t \in \mathcal{T}$, zone $z \in \mathcal{Z}$ and node $\omega \in \Omega_{\sigma_t}$
$x_{\omega,z,t,k}^{\text{NM,CP}}$	Amount of new material $k \in \mathcal{K} \setminus \mathcal{K}^{\text{CP}}$ used in cathode production in time period $t \in \mathcal{T}$, zone $z \in \mathcal{Z}$ and node $\omega \in \Omega_{\sigma_t}$
$x_{\omega,z,t,k}^{\text{NM,NB}}$	Amount of new material $k \in \mathcal{K}$ used to produce new batteries in time period $t \in \mathcal{T}$, zone $z \in \mathcal{Z}$ and node $\omega \in \Omega_{\sigma_t}$
$x_{\omega,z,t,i}^{\text{RB}}$	Amount of retired battery of chemistry $i \in \mathcal{I}$ in inventory in time period $t \in \mathcal{T}$, zone $z \in \mathcal{Z}$ and node $\omega \in \Omega_{\sigma_t}$
$x_{\omega,z,t,i,j}^{\text{RB,RM}}$	Amount of retired battery of chemistry $i \in \mathcal{I}$ recycled with process $j \in \mathcal{J}$ in time period $t \in \mathcal{T}$, zone $z \in \mathcal{Z}$ and node $\omega \in \Omega_{\sigma_t}$
$x_{\omega,z,t,k}^{\text{RM,INV}}$	Amount of output material $k \in \mathcal{K}$ from battery recycling put in inventory in time period $t \in \mathcal{T}$, zone $z \in \mathcal{Z}$ and node $\omega \in \Omega_{\sigma_t}$
$x_{\omega,z,t,k}^{\text{RM,S}}$	Amount of output material $k \in \mathcal{K}$ from battery recycling sold to the market in time period $t \in \mathcal{T}$, zone $z \in \mathcal{Z}$ and node $\omega \in \Omega_{\sigma_t}$

$x_{\omega,z,z',t,i}^{\text{TR,RB}}$	Amount of retired battery with chemistry $i \in \mathcal{I}$ transported from zone $z \in \mathcal{Z}$ to zone $z' \in \mathcal{Z} \setminus \{z\}$ in time period $t \in \mathcal{T}$ and node $\omega \in \Omega_{\sigma_t}$
$x_{\omega,z,z',t,k}^{\text{TR,RM}}$	Amount of recycled material $k \in \mathcal{K}$ transported from zone $z \in \mathcal{Z}$ to zone $z' \in \mathcal{Z} \setminus \{z\}$ in time period $t \in \mathcal{T}$ and node $\omega \in \Omega_{\sigma_t}$
$y_{z,l,k,n}^{\text{CP}}$	Annual capacity of cathode production line $n \in \mathcal{N}_{l,k}^{\text{CP}}$ producing material $k \in \mathcal{K}^{\text{CP}}$ in zone $z \in \mathcal{Z}$ during planning period $l \in \mathcal{L}$
$y_{z,l,j,n}^{\text{REC}}$	Annual capacity of recycling process $j \in \mathcal{J}$ at facility $n \in \mathcal{N}_l^{\text{REC}}$ in zone $z \in \mathcal{Z}$ during planning period $l \in \mathcal{L}$
$y_{z,l,k}^{\text{CP}}$	Number of cathode production lines producing material $k \in \mathcal{K}^{\text{CP}}$ in zone $z \in \mathcal{Z}$ during planning period $l \in \mathcal{L}$ with capacity at the upper bound u^{CP}
$y_{z,l,j}^{\text{REC}}$	Number of facilities in zone $z \in \mathcal{Z}$ during planning period $l \in \mathcal{L}$ with capacity for recycling process $j \in \mathcal{J}$ at the upper bound u^{REC}
$y_{z,l,k,+}^{\text{CP}}$	Annual capacity of the cathode production line producing material $k \in \mathcal{K}^{\text{CP}}$ in zone $z \in \mathcal{Z}$ during planning period $l \in \mathcal{L}$ that does not have capacity at its upper or lower bound
$y_{z,l,j,+}^{\text{REC}}$	Annual capacity of the recycling facility for process $j \in \mathcal{J}$ in zone $z \in \mathcal{Z}$ during planning period $l \in \mathcal{L}$ that does not have capacity at its upper or lower bound

A.2 Battery Mass Parameter Calculation

The parameter $m_{\xi,t,i}$ gives the average mass of a new battery by year, demand scenario, and chemistry, accounting for differences in battery size between BEVs and PHEVs. Let BEV_t^{SDS} and BEV_t^{STEPS} represent the proportion of EV stock composed of BEVs under the SDS and STEPS projections, respectively, using data from Xu et al. (2020). Note that $1 - BEV_t^{\text{SDS}}$ gives the proportion composed of PHEVs. Similarly to the scenario-adjusted cost distribution parameters $(v_{\xi,t,m}^{\text{MED}}, v_{\xi,t,m}^{\text{LB}}, v_{\xi,t,m}^{\text{UB}})$, we compute samples for BEV_t from the scenario multipliers $\lambda_{\xi,t}$:

$$BEV_{\xi,t} = BEV_t^{\text{SDS}} \lambda_{\xi,t} + BEV_t^{\text{STEPS}} (1 - \lambda_{\xi,t}).$$

We then convert the proportion of battery stock $BEV_{\xi,t}$ to a proportion of new battery sales $\overline{BEV}_{\xi,t}$ recursively by

$$\overline{BEV}_{\xi,t} = \frac{BEV_{\xi,t} EV_{\xi,t} - BEV_{\xi,t-1} EV_{\xi,t-1} + \sum_{a=1}^A \overline{BEV}_{\xi,t-a} LS_a AB_{\xi,t,a}}{AB_{\xi,t,0}}.$$

Note that historical BEV proportions are available through year $-A$. Let m_i^{BEV} and m_i^{PHEV} be the average mass of BEV and PHEV batteries for each chemistry (Xu et al. 2020). The average mass of a new battery is then computed

$$m_{\xi,t,i} = m_i^{\text{BEV}} \overline{BEV}_{\xi,t} + m_i^{\text{PHEV}} (1 - \overline{BEV}_{\xi,t}).$$

A.3 Sensitivity to Zonal Cost Parameters

Cost parameters vary across zone due to differences in seven location-dependent costs: labor, electricity, natural gas, water, landfill, wastewater, and an equipment cost multiplier. All planning and operational cost objects that are indexed by zone are functions of these values. Table A.4 gives the baseline values for these parameters from the EverBatt model (Dai et al. 2019).

To investigate the robustness of our model and reported solutions against these parameters, we perform a sensitivity analysis on Case 2, variation DR1. We perturb the baseline value for each parameter in the U.S. and China individually by $\pm 10\%$, $\pm 20\%$, and $\pm 40\%$, and report the relative change in objective value and in installed

	U.S.	China
Equipment Cost Multiplier (%)	100	60
Labor (\$/hr)	20.00	3.00
Electricity (\$/MWh)	68.00	88.00
Natural Gas (\$/MMBtu)	3.84	12.00
Water (\$/1000 gal)	5.00	2.00
Landfill (\$/ton)	55.36	10.00
Wastewater (\$/1000 gal)	7.00	3.00

Table A.4: Baseline values for location-dependent cost parameters by zone.

capacity for recycling and cathode production facilities. For baseline solution \bar{y} and solution y from the perturbed model, the relative change in recycling capacity for zone z is computed by

$$100 \times \frac{\sum_{j \in \mathcal{J}, l \in \mathcal{L}} u^{\text{REC}} (\bar{y}_{z,l,j}^{\text{REC}} - y_{z,l,j}^{\text{REC}}) + \bar{y}_{z,l,j,+}^{\text{REC}} - y_{z,l,j,+}^{\text{REC}}}{\sum_{j \in \mathcal{J}, l \in \mathcal{L}, z' \in \mathcal{Z}} u^{\text{REC}} \bar{y}_{z',l,j}^{\text{REC}} + \bar{y}_{z',l,j,+}^{\text{REC}}}.$$

Relative changes in cathode production capacity are computed analogously.

Table A.5 reports the relative change in objective value for parameters that yield changes over 0.05% for some tested perturbation. The optimal objective is very stable against perturbations to the location-dependent cost parameters. In fact, perturbations to only two of the 14 parameters cause objective changes above 0.05%, namely, the labor cost and equipment cost multiplier in China. The optimal objective is most sensitive to these parameters, although the relative change never exceeds $\pm 1\%$.

Tables A.6a and A.6b give the relative change in recycling and cathode production capacity, respectively, under each parameter perturbation. Some differences in the reported optimal solutions may be attributed to the use of a 0.01% relative optimality tolerance in the objective value, which potentially enforces a weaker tolerance in the solution space. In general, the solutions show a decrease in U.S. capacity and an increase in China capacity when cost parameters increase in the U.S., and the opposite trends when cost parameters increase in China. The recycling solution is more stable against perturbations than the cathode production solution. Relative changes in recycling capacity generally do not exceed 10%, even when the cost parameters are perturbed by $\pm 40\%$. Cathode production capacity never changes more than 0.5% in the U.S., meaning that under all parameter perturbations, almost no U.S. cathode production capacity is constructed. On the other hand, cathode production capacity in China exhibits higher sensitivity, varying by up to 67% from the baseline solution. This result suggests that, as the objective value remains stable, there are many near-optimal cathode production solutions that yield similar objective values. Both recycling and cathode production solutions are most sensitive to labor cost and the equipment cost multiplier. Perturbations to the other cost parameters never cause large changes in the capacity solutions. Overall, these results show that our recycling capacity solution is resilient to changes in location-dependent cost parameters, and the cathode production capacity solution is resilient to changes in all location-dependent cost parameters except the equipment cost multiplier in China.

A.4 Proofs of Results

Proposition 1. *For any $\bar{y} \geq 0$ that satisfies (3c)-(3f), $\{(y, x) \geq 0 : (1), (2), (3), y = \bar{y}\} \neq \emptyset$.*

Proof. Fix $y \geq 0$ so that (3c)-(3f) are satisfied. We construct a corresponding feasible x that only buys new materials to manufacture batteries and does not recycle. Take $x_{\omega,z,t,k}^{\text{NM,NB}} = \sum_{i \in \mathcal{I}} \Delta_{i,k}^{\text{NB}} d_{\omega,z,t,i}$. Further, set $x_{\omega,z,t,i}^{\text{RB}} = \sum_{t'=1}^t s_{a_{\omega}(t'),z,t',i}$ and $x_{\omega,z,0,i}^{\text{RB}} = 0$. Note that $a_{\omega}(t) = \omega$ for $\omega \in \Omega_{\sigma_t}$. Set all other components of x to 0. Because battery supply s , demand d , and material requirements Δ are nonnegative under Assumption 1, $x \geq 0$.

Zone	Parameter	Perturbation					
		-40%	-20%	-10%	+10%	+20%	+40%
China	Equipment	-0.7%	-0.3%	-0.1%	0.1%	0.2%	0.4%
	Labor	-0.1%	0.0%	0.0%	0.0%	0.0%	0.1%

Table A.5: Relative change in optimal objective value under select location-dependent cost parameter perturbations. All other perturbations yield relative changes under 0.05%.

Zone	Parameter	Perturbation											
		-40%		-20%		-10%		+10%		+20%		+40%	
		U.S.	C.N.	U.S.	C.N.	U.S.	C.N.	U.S.	C.N.	U.S.	C.N.	U.S.	C.N.
U.S.	Equipment	9.7	-8.6	5.5	-4.4	3.8	-2.7	-2.4	3.2	-2.4	3.3	-2.4	3.7
	Labor	10.0	-9.8	3.5	-2.5	3.4	-2.7	-2.3	3.4	-2.4	3.6	-2.4	3.7
	Electricity	3.9	-2.3	5.1	-4.6	5.4	-2.2	0.2	-0.6	-2.4	2.7	-2.4	3.0
	Natural Gas	0.5	0.7	1.3	0.5	0.0	1.3	1.0	0.3	0.5	0.6	1.1	0.0
	Water	-1.3	1.0	0.0	2.6	0.3	0.2	0.8	-0.1	1.3	-0.4	-0.8	1.8
	Landfill	0.2	1.4	2.3	-1.1	0.5	1.2	3.2	-2.4	1.6	-0.1	-1.3	2.2
	Wastewater	2.4	-0.8	1.9	-0.7	2.4	-2.7	-0.8	1.7	-0.1	1.5	0.3	1.0
China	Equipment	-2.4	6.4	-2.4	6.9	-1.3	3.4	4.9	-4.9	5.6	-7.5	8.9	-11.2
	Labor	-2.4	3.1	2.1	-1.2	0.9	1.3	3.0	-2.9	0.3	0.8	1.3	-2.7
	Electricity	-2.4	3.4	-2.1	3.6	-0.3	1.7	2.1	-2.8	4.8	-4.5	5.4	-4.6
	Natural Gas	0.3	1.4	0.3	0.5	0.5	0.7	2.5	-1.8	4.6	-3.4	-1.1	2.2
	Water	1.5	-0.3	1.2	-1.3	0.5	0.8	0.8	-0.8	3.0	-2.1	0.8	1.3
	Landfill	0.3	2.4	-1.3	2.6	0.0	2.0	2.6	-2.1	0.5	-0.7	1.6	-1.2
	Wastewater	0.0	-0.6	0.8	-1.5	1.1	0.0	2.7	-1.4	0.3	1.4	1.3	0.0

(a) Relative change (%) to recycling capacity under cost parameter perturbations.

Zone	Parameter	Perturbation											
		-40%		-20%		-10%		+10%		+20%		+40%	
		U.S.	C.N.	U.S.	C.N.	U.S.	C.N.	U.S.	C.N.	U.S.	C.N.	U.S.	C.N.
U.S.	Equipment	0.3	0.4	0.0	-3.8	0.0	-1.4	0.0	-3.8	0.0	-2.1	0.0	-5.4
	Labor	0.0	-2.4	0.0	-3.4	0.0	-3.7	0.0	-3.5	0.0	-4.6	0.0	5.8
	Electricity	0.0	-4.5	0.0	-1.1	0.3	-3.7	0.0	-0.7	0.0	3.4	0.0	1.4
	Natural Gas	0.0	-4.7	0.0	-1.1	0.0	-6.8	0.0	-3.0	0.0	-2.1	0.3	-4.8
	Water	0.0	-0.3	0.0	1.4	0.0	0.4	0.0	0.8	0.0	-4.9	0.0	3.8
	Landfill	0.0	1.6	0.0	-4.1	0.1	-5.0	0.0	-2.3	0.0	-1.2	0.0	-0.2
	Wastewater	0.1	-1.4	0.0	-2.4	0.0	0.9	0.0	2.7	0.0	6.2	0.0	0.0
China	Equipment	0.0	66.1	0.0	30.1	0.0	13.0	0.0	-19.2	0.0	-27.6	0.0	-67.1
	Labor	0.0	9.1	0.0	3.1	0.3	0.8	0.0	-0.6	0.0	2.7	0.0	-10.5
	Electricity	0.0	-1.2	0.0	0.1	0.0	-3.0	0.0	-1.7	0.0	-1.2	0.0	-1.4
	Natural Gas	0.0	-1.0	0.0	1.7	0.3	2.8	0.0	-0.7	0.0	-4.0	0.0	-6.0
	Water	0.0	0.2	0.0	-0.3	0.0	-1.7	0.0	2.1	0.0	-4.1	0.0	-1.4
	Landfill	0.0	0.7	0.3	2.8	0.0	-2.3	0.0	-0.7	0.0	-4.0	0.0	0.7
	Wastewater	0.0	1.3	0.0	-3.8	0.0	-4.9	0.4	-0.5	0.0	-5.6	0.0	2.8

(b) Relative change (%) to cathode production capacity under cost parameter perturbations.

Table A.6: Sensitivity of optimal facility capacity in the U.S. and China (C.N.) to perturbations in zonal cost parameters. Each row gives results for perturbations to one parameter in one zone.

The construction of $x^{\text{NM,NB}}$ ensures that (1a) and (1b) are satisfied, and that of x^{RB} ensures that (2c) is satisfied. The remainder of constraints in (1) and (2) only involve components of x that are 0 and are thus satisfied. As $y \geq 0$, the solution x is feasible for (3a) and (3b). Thus, given y , we can construct $x \geq 0$ so that constraints (1)-(3) are satisfied. \square

Lemma A.1 (Horst et al. (2000), Theorem 1.19). *Let \mathcal{X} be a bounded polytope and $f : \mathcal{X} \rightarrow \mathbb{R}$ be a concave function. Then, f attains its minimum at an extreme point of \mathcal{X} .*

Proof. Let $\{x^{(j)}\}_{j=1}^J$ be the extreme points of \mathcal{X} . As \mathcal{X} is bounded, $\mathcal{X} = \text{conv}\{x^{(j)}\}_{j=1}^J$. Then, for any $x \in \mathcal{X}$, there is some $\lambda \geq 0$ with $\sum_{j=1}^J \lambda_j = 1$ and $\sum_{j=1}^J \lambda_j x^{(j)} = x$. By concavity of f ,

$$f(x) = f\left(\sum_{j=1}^J \lambda_j x^{(j)}\right) \geq \sum_{j=1}^J \lambda_j f(x^{(j)}) \geq \min_{j \in [J]} f(x^{(j)}) \left(\sum_{j=1}^J \lambda_j\right) = \min_{j \in [J]} f(x^{(j)}).$$

Therefore, f achieves its minimum on \mathcal{X} at some element of $\{x^{(j)}\}_{j=1}^J$, which is an extreme point of \mathcal{X} . \square

Lemma A.2. *Let f be a concave function and $\mathcal{X} \subseteq \mathbb{R}_+^p$ be a nonempty polyhedron. Then, if $\inf_{x \in \mathcal{X}} f(x) > -\infty$, it attains a finite optimal solution at an extreme point of \mathcal{X} .*

Proof. Suppose $\inf_{x \in \mathcal{X}} f(x) > -\infty$. Let $\{x^{(j)}\}_{j=1}^J$ and $\{r^{(k)}\}_{k=1}^K$ be the extreme points and extreme rays of \mathcal{X} , and denote $\epsilon = \inf_{x \in \mathcal{X}} f(x)$, which is finite as the problem is feasible. Note that

$$\mathcal{X} = \text{conv}\{x^{(j)}\}_{j=1}^J + \text{cone}\{r^{(k)}\}_{k=1}^K.$$

Further, as $\mathcal{X} \subseteq \mathbb{R}_+^p$, it does not contain a line, which implies that it has at least one extreme point.

Select any $x \in \text{conv}\{x^{(j)}\}_{j=1}^J$ and $r \in \text{cone}\{r^{(k)}\}_{k=1}^K$. To prove by contradiction, suppose that $f(x+r) < f(x)$. Take $\delta = \frac{f(x)-\epsilon+1}{f(x)-f(x+r)}$ and note that $\delta \geq 1$ as $\epsilon \leq f(x+r)$. Then, by concavity of f ,

$$f(x+r) = f\left(\frac{1}{\delta}(x+\delta r) + \frac{\delta-1}{\delta}x\right) \geq \frac{1}{\delta}f(x+\delta r) + \frac{\delta-1}{\delta}f(x),$$

and

$$f(x+\delta r) \leq \delta(f(x+r) - f(x)) + f(x) = \epsilon - 1.$$

As $x+\delta r \in \mathcal{X}$, this contradicts the definition of ϵ , and thus $f(x) \leq f(x+r)$. This shows that

$$\inf_{x \in \mathcal{X}} f(x) = \inf_{x \in \text{conv}\{x^{(j)}\}_{j=1}^J} f(x).$$

The latter is a concave minimization over a bounded polytope, and thus attains its optimal value ϵ at an extreme point of $\text{conv}\{x^{(j)}\}_{j=1}^J$ by Lemma A.1. Extreme points of the convex hull of a discrete set are elements of the set, and these elements are extreme points of \mathcal{X} . Thus, the optimal value ϵ is obtained at an extreme point of \mathcal{X} . \square

Proposition 2. *The model (P) is feasible and has an optimal solution at an extreme point of its feasible region.*

Proof. We first establish that (P) is feasible. Take $y = 0$. As $u^{\text{REC}} > 0$ and $u^{\text{CP}} > 0$ under Assumption 1, y is feasible for (3c)-(3f). By Proposition 1, there is some $x \geq 0$ so that (y, x) satisfies (1), (2), and (3). Then, (y, x) is feasible for (P).

Next, consider the relaxation of (P):

$$\begin{aligned}
& \min_{x,y} \sum_{t \in \mathcal{T}} (1-\gamma)^{t-1} \left(C_t^{\text{PL}}(y) + \sum_{\omega \in \Omega_{\sigma_t}} p_{\omega} C_{\omega,t}^{\text{OP}}(x) \right) \\
& \text{s.t.} \quad (1\text{e}), (2\text{a}), (2\text{c}) \\
& \quad x \geq 0, y \geq 0.
\end{aligned} \tag{A.1}$$

Any feasible solution for (P) is feasible for (A.1) with the same objective value. Note that, as constraints (3) are relaxed, there are no constraints coupling variables x and y . Thus, (A.1) is equivalent to

$$\begin{aligned}
& \min_{y \geq 0} \sum_{t \in \mathcal{T}} (1-\gamma)^{t-1} C_t^{\text{PL}}(y) + \min_{x \geq 0} \sum_{t \in \mathcal{T}} (1-\gamma)^{t-1} \sum_{\omega \in \Omega_{\sigma_t}} p_{\omega} C_{\omega,t}^{\text{OP}}(x) \\
& \text{s.t.} \quad (1\text{e}), (2\text{a}), (2\text{c}).
\end{aligned} \tag{A.2}$$

As C_t^{PL} is monotonic increasing in each variable y by Assumption 1, $y = 0$ is optimal for the first problem of (A.2).

Consider any direction $x \geq 0$ in which the feasible region of the second problem of (A.2) is unbounded. By (2c),

$$x_{\omega,z,t,i}^{\text{RB}} - x_{a_{\omega}(t-1),z,t-1,i}^{\text{RB}} + \sum_{j \in \mathcal{J}} x_{\omega,z,t,i,j}^{\text{RB,RM}} - \sum_{z' \in \mathcal{Z} \setminus \{z\}} (x_{\omega,z',z,t,i}^{\text{TR,RB}} - x_{\omega,z,z',t,i}^{\text{TR,RB}}) = 0.$$

Summing over z yields $\sum_{z \in \mathcal{Z}} (x_{\omega,z,t,i}^{\text{RB}} - x_{a_{\omega}(t-1),z,t-1,i}^{\text{RB}} + \sum_{j \in \mathcal{J}} x_{\omega,z,t,i,j}^{\text{RB,RM}}) = 0$. As $x_{\omega,z,0,i}^{\text{RB}} = 0$ and $x \geq 0$, by induction $x^{\text{RB}} = 0$ and $x^{\text{RB,RM}} = 0$. Then, (1e) gives $x_{\omega,z,t,k}^{\text{RM,INV}} + x_{\omega,z,t,k}^{\text{RM,S}} - \sum_{i \in \mathcal{I}, j \in \mathcal{J}} \Delta_{k,i,j}^{\text{REC}} x_{\omega,z,t,i,j}^{\text{RB,RM}} = 0$, so $x^{\text{RM,INV}} = 0$ and $x^{\text{RM,S}} = 0$ as $x \geq 0$.

Then, consider the change in objective in direction x , given by $\sum_{t \in \mathcal{T}} (1-\gamma)^{t-1} \sum_{\omega \in \Omega_{\sigma_t}} p_{\omega} C_{\omega,t}^{\text{OP}}(x)$. As $\gamma < 1$, $c \geq 0$, $v \geq 0$, $p \geq 0$, $x \geq 0$, and $x^{\text{RM,S}} = 0$, it holds that $\sum_{t \in \mathcal{T}} (1-\gamma)^{t-1} \sum_{\omega \in \Omega_{\sigma_t}} p_{\omega} C_{\omega,t}^{\text{OP}}(x) \geq 0$, and the direction does not improve the objective. As the second problem of (A.2) is a linear program, this proves that its objective is bounded. Thus, neither problem in (A.2) is unbounded, so (A.1) and (P) are bounded in objective. As (P) is a concave minimization over a polyhedron contained in the nonnegative orthant and is bounded in objective, it attains its optimal value at an extreme point of its feasible region by Lemma A.2. \square

Theorem 1. *Let (\tilde{y}, \tilde{x}) be an extreme point of $\{(y, x) \geq 0 : (1), (2), (3)\}$. Then, \tilde{y}^{REC} satisfies (6) and \tilde{y}^{CP} satisfies the corresponding property.*

Proof. The comparable solution structure for \tilde{y}^{CP} with total capacity $Y_{z,l,k} = \sum_{n \in \mathcal{N}_{l,k}^{\text{CP}}} \tilde{y}_{z,l,k,n}^{\text{CP}}$ is given by

$$\begin{aligned}
\mathcal{C}(\{\tilde{y}_{z,l,k,n}^{\text{CP}}\}_{n \in \mathcal{N}_{l,k}^{\text{CP}}}; u^{\text{CP}}) & \geq \left\lceil \frac{Y_{z,l,k}}{u^{\text{CP}}} \right\rceil - 1; \\
\mathcal{C}(\{\tilde{y}_{z,l,k,n}^{\text{CP}}\}_{n \in \mathcal{N}_{l,k}^{\text{CP}}}; 0) & \geq |\mathcal{N}_{l,k}^{\text{CP}}| - \left\lceil \frac{Y_{z,l,k}}{u^{\text{CP}}} \right\rceil \quad \forall k \in \mathcal{K}^{\text{CP}}, l \in \mathcal{L}, z \in \mathcal{Z}.
\end{aligned} \tag{A.3}$$

We demonstrate the result only for the property of the recycling capacity solution \tilde{y}^{REC} , as the same arguments apply to the cathode production capacity solution \tilde{y}^{CP} . The result is shown by contraposition. Denote the polyhedron $\mathcal{X} = \{(y, x) \geq 0 : (1), (2), (3)\}$ and consider any $(y, x) \in \mathcal{X}$. Fix some z, l, j and let the total recycling capacity be $Y_{z,l,j} = \sum_{n \in \mathcal{N}_l^{\text{REC}}} y_{z,l,j,n}^{\text{REC}}$. Suppose that (6) does not hold for y^{REC} .

First, consider the case where $\mathcal{C}(\{y_{z,l,j,n}^{\text{REC}}\}_{n \in \mathcal{N}_l^{\text{REC}}}; u^{\text{REC}}) \leq \left\lceil \frac{Y_{z,l,j}}{u^{\text{REC}}} \right\rceil - 2$. Suppose for contradiction that there are one or fewer indices n with $u^{\text{REC}} > y_{z,l,j,n}^{\text{REC}} > 0$. Then, the total number of indices corresponding to nonzero

elements is bounded by $\left\lceil \frac{Y_{z,l,j}}{u^{\text{REC}}} \right\rceil - 1$, and

$$\sum_{n \in \mathcal{N}_l^{\text{REC}}} y_{z,l,j,n}^{\text{REC}} \leq u^{\text{REC}} \left(\left\lceil \frac{Y_{z,l,j}}{u^{\text{REC}}} \right\rceil - 1 \right) < Y_{z,l,j} = \sum_{n \in \mathcal{N}_l^{\text{REC}}} y_{z,l,j,n}^{\text{REC}}.$$

By this contradiction, there must be at least two indices n_1, n_2 with $u^{\text{REC}} > y_{z,l,j,n}^{\text{REC}} > 0$ for $n \in \{n_1, n_2\}$.

Second, consider the case where $\mathcal{C}(\{y_{z,l,j,n}^{\text{REC}}\}_{n \in \mathcal{N}_l^{\text{REC}}}; 0) \leq |\mathcal{N}_l^{\text{REC}}| - \left\lceil \frac{Y_{z,l,j}}{u^{\text{REC}}} \right\rceil - 1$. Again, suppose for contradiction that there are one or fewer indices n with $u^{\text{REC}} > y_{z,l,j,n}^{\text{REC}} > 0$. Then, there are at least $\left\lceil \frac{Y_{z,l,j}}{u^{\text{REC}}} \right\rceil$ elements at the upper bound u^{REC} and one additional nonzero element (that may also take the value u^{REC}), so

$$\sum_{n \in \mathcal{N}_l^{\text{REC}}} y_{z,l,j,n}^{\text{REC}} > u^{\text{REC}} \left\lceil \frac{Y_{z,l,j}}{u^{\text{REC}}} \right\rceil \geq Y_{z,l,j} = \sum_{n \in \mathcal{N}_l^{\text{REC}}} y_{z,l,j,n}^{\text{REC}}.$$

By this contradiction, there must again be at least two indices n_1, n_2 with $u^{\text{REC}} > y_{z,l,j,n}^{\text{REC}} > 0$ for $n \in \{n_1, n_2\}$.

In either scenario, select such indices n_1, n_2 , and denote

$$\delta = \min\{y_{z,l,j,n_1}^{\text{REC}}, y_{z,l,j,n_2}^{\text{REC}}, u^{\text{REC}} - y_{z,l,j,n_1}^{\text{REC}}, u^{\text{REC}} - y_{z,l,j,n_2}^{\text{REC}}\}.$$

By construction, $\delta > 0$. We construct perturbed solutions

$$\bar{y}_{z,l,j,n}^{\text{REC}}(1) = \begin{cases} y_{z,l,j,n}^{\text{REC}} & n \notin \{n_1, n_2\} \\ y_{z,l,j,n}^{\text{REC}} + \delta & n = n_1 \\ y_{z,l,j,n}^{\text{REC}} - \delta & n = n_2, \end{cases}$$

and

$$\bar{y}_{z,l,j,n}^{\text{REC}}(2) = \begin{cases} y_{z,l,j,n}^{\text{REC}} & n \notin \{n_1, n_2\} \\ y_{z,l,j,n}^{\text{REC}} - \delta & n = n_1 \\ y_{z,l,j,n}^{\text{REC}} + \delta & n = n_2. \end{cases}$$

Let $\bar{y}^{\text{CP}}(1) = \bar{y}^{\text{CP}}(2) = y^{\text{CP}}$. By construction, $0 \leq \bar{y}_{z,l,j,n}^{\text{REC}}(1) \leq u^{\text{REC}}$ and $\sum_{n \in \mathcal{N}_l^{\text{REC}}} \bar{y}_{z,l,j,n}^{\text{REC}}(1) = \sum_{n \in \mathcal{N}_l^{\text{REC}}} y_{z,l,j,n}^{\text{REC}}$, so $(\bar{y}(1), x)$ satisfies all constraints of \mathcal{X} . Similarly, $(\bar{y}(2), x) \in \mathcal{X}$. Finally, we note that $(y, x) = \frac{1}{2}(\bar{y}(1), x) + \frac{1}{2}(\bar{y}(2), x)$, so (y, x) is a convex combination of other points in \mathcal{X} , and thus is not an extreme point.

This shows that, if a solution y^{REC} does not satisfy (6), then the solution (y, x) is not an extreme point of \mathcal{X} . Thus, the contrapositive of this result is also true, namely, an extreme point (\tilde{y}, \tilde{x}) of \mathcal{X} must satisfy (6). By similar logic, it can be shown that an extreme point must also satisfy (A.3). □

Theorem 2. *The models (P) and (PMI) have the same optimal objective value.*

Proof. We first demonstrate that a feasible solution for (PMI) can be mapped to an equivalent feasible solution for (P). Let (\bar{y}, \bar{x}) be feasible for (PMI). We define \tilde{y} by

$$\tilde{y}_{z,l,j,n}^{\text{REC}} = \begin{cases} u^{\text{REC}} & n \leq \bar{y}_{z,l,j}^{\text{REC}} \\ \bar{y}_{z,l,j,+}^{\text{REC}} & n = \bar{y}_{z,l,j}^{\text{REC}} + 1 \\ 0 & \text{otherwise,} \end{cases}$$

$$\tilde{y}_{z,l,k,n}^{\text{CP}} = \begin{cases} u^{\text{CP}} & n \leq \bar{y}_{z,l,k}^{\text{CP}} \\ \bar{y}_{z,l,k,+}^{\text{CP}} & n = \bar{y}_{z,l,k}^{\text{CP}} + 1 \\ 0 & \text{otherwise.} \end{cases}$$

By construction, $0 \leq \tilde{y}_{z,l,j,n}^{\text{REC}} \leq u^{\text{REC}}$ and $0 \leq \tilde{y}_{z,l,k,n}^{\text{CP}} \leq u^{\text{CP}}$. Further, $\sum_{n \in \mathcal{N}_l^{\text{REC}}} \tilde{y}_{z,l,j,n}^{\text{REC}} = u^{\text{REC}} \bar{y}_{z,l,j}^{\text{REC}} + \bar{y}_{z,l,j,+}^{\text{REC}}$ and similarly $\sum_{n \in \mathcal{N}_{l,k}^{\text{CP}}} \tilde{y}_{z,l,k,n}^{\text{CP}} = u^{\text{CP}} \bar{y}_{z,l,k}^{\text{CP}} + \bar{y}_{z,l,k,+}^{\text{CP}}$. Due to feasibility of (\bar{y}, \bar{x}) for (7), the solution (\tilde{y}, \bar{x}) is feasible for constraints (3). Further, \bar{x} remains feasible for (1) and (2). Thus, (\tilde{y}, \bar{x}) is feasible for (P). The objective values satisfy

$$\begin{aligned} C_t^{\text{PL}}(\tilde{y}) &= \sum_{z \in \mathcal{Z}} \left(\sum_{j \in \mathcal{J}} \sum_{n \in \mathcal{N}_{l,j}^{\text{REC}}} f_{z,j}^{\text{REC}}(\tilde{y}_{z,l,j,n}^{\text{REC}}) + \sum_{k \in \mathcal{K}^{\text{CP}}} \sum_{n \in \mathcal{N}_{l,k}^{\text{CP}}} f_{z,k}^{\text{CP}}(\tilde{y}_{z,l,k,n}^{\text{CP}}) \right) \\ &= \sum_{z \in \mathcal{Z}} \left(\sum_{j \in \mathcal{J}} (\bar{y}_{z,l,j}^{\text{REC}} f_{z,j}^{\text{REC}}(u^{\text{REC}}) + f_{z,j}^{\text{REC}}(\bar{y}_{z,l,j,+}^{\text{REC}})) + \sum_{k \in \mathcal{K}^{\text{CP}}} (\bar{y}_{z,l,k}^{\text{CP}} f_{z,k}^{\text{CP}}(u^{\text{CP}}) + f_{z,k}^{\text{CP}}(\bar{y}_{z,l,k,+}^{\text{CP}})) \right) \\ &= \bar{C}_t^{\text{PL}}(\bar{y}), \end{aligned}$$

as $f(0) = 0$. Thus (\tilde{y}, \bar{x}) has the same objective value in (P) as (\bar{y}, \bar{x}) in (PMI).

In the opposite direction, we consider an optimal solution for (P) that occurs at an extreme point of its feasible region, which exists by Proposition 2. Denote this optimal extreme point (\tilde{y}, \tilde{x}) . By Theorem 1, this solution satisfies (6) and (A.3).

As $u^{\text{REC}} > 0$ under Assumption 1, each index $n \in \mathcal{N}_l^{\text{REC}}$ can be counted by at most one of $\mathcal{C}(\{\tilde{y}_{z,l,j,n}^{\text{REC}}\}_{n \in \mathcal{N}_l^{\text{REC}}}; 0)$ and $\mathcal{C}(\{\tilde{y}_{z,l,j,n}^{\text{REC}}\}_{n \in \mathcal{N}_l^{\text{REC}}}; u^{\text{REC}})$. By this property and the structure (6),

$$|\mathcal{N}_l^{\text{REC}}| \geq \mathcal{C}(\{\tilde{y}_{z,l,j,n}^{\text{REC}}\}_{n \in \mathcal{N}_l^{\text{REC}}}; 0) + \mathcal{C}(\{\tilde{y}_{z,l,j,n}^{\text{REC}}\}_{n \in \mathcal{N}_l^{\text{REC}}}; u^{\text{REC}}) \geq |\mathcal{N}_l^{\text{REC}}| - 1.$$

If the lower bound holds with equality, we can select the unique $\bar{n}_{z,l,j}$ so that $0 < \tilde{y}_{z,l,j,(\bar{n}_{z,l,j})}^{\text{REC}} < u^{\text{REC}}$. Otherwise, we select arbitrary $\bar{n}_{z,l,j}$. The index has the property that $\tilde{y}_{z,l,j,n}^{\text{REC}} \in \{0, u^{\text{REC}}\}$ for any $n \neq \bar{n}_{z,l,j}$. We can similarly select $\bar{n}_{z,l,k}$ for \tilde{y}^{CP} . Now, we define

$$\begin{aligned} \bar{y}_{z,l,j}^{\text{REC}} &= \mathcal{C}(\{\tilde{y}_{z,l,j,n}^{\text{REC}}\}_{n \in \mathcal{N}_l^{\text{REC}} \setminus \{\bar{n}_{z,l,j}\}}; u^{\text{REC}}); \\ \bar{y}_{z,l,j,+}^{\text{REC}} &= \tilde{y}_{z,l,j,\bar{n}_{z,l,j}}^{\text{REC}}; \\ \bar{y}_{z,l,k}^{\text{CP}} &= \mathcal{C}(\{\tilde{y}_{z,l,k,n}^{\text{CP}}\}_{n \in \mathcal{N}_{l,k}^{\text{CP}} \setminus \{\bar{n}_{z,l,k}\}}; u^{\text{REC}}); \text{ and} \\ \bar{y}_{z,l,k,+}^{\text{CP}} &= \tilde{y}_{z,l,k,\bar{n}_{z,l,k}}^{\text{CP}}. \end{aligned}$$

By construction, $\bar{y}_{z,l,j}^{\text{REC}}$ and $\bar{y}_{z,l,k}^{\text{CP}}$ satisfy the integrality constraints (7e) and (7f), and further $\bar{y}_{z,l,j,+}^{\text{REC}}$ and $\bar{y}_{z,l,k,+}^{\text{CP}}$ satisfy nonnegativity and the upper bounds (7g) and (7h) by the feasibility of \tilde{y} for (P). By definition of \bar{n} ,

$$\sum_{n \in \mathcal{N}_l^{\text{REC}}} \tilde{y}_{z,l,j,n}^{\text{REC}} = u^{\text{REC}} \mathcal{C}(\{\tilde{y}_{z,l,j,n}^{\text{REC}}\}_{n \in \mathcal{N}_l^{\text{REC}} \setminus \{\bar{n}_{z,l,j}\}}; u^{\text{REC}}) + \tilde{y}_{z,l,j,(\bar{n}_{z,l,j})}^{\text{REC}} = u^{\text{REC}} \bar{y}_{z,l,j}^{\text{REC}} + \bar{y}_{z,l,j,+}^{\text{REC}},$$

and similarly

$$\sum_{n \in \mathcal{N}_{l,k}^{\text{CP}}} \tilde{y}_{z,l,k,n}^{\text{CP}} = u^{\text{CP}} \bar{y}_{z,l,k}^{\text{CP}} + \bar{y}_{z,l,k,+}^{\text{CP}}.$$

Thus, feasibility of (\tilde{y}, \tilde{x}) for (3) implies that (\bar{y}, \tilde{x}) is feasible for (7a)-(7d), and \tilde{x} remains feasible for (1) and (2). Thus, (\bar{y}, \tilde{x}) is feasible for (PMI). Considering the objective,

$$\begin{aligned} \sum_{n \in \mathcal{N}_l^{\text{REC}}} f_{z,j}^{\text{REC}}(\tilde{y}_{z,l,j,n}^{\text{REC}}) &= \mathcal{C}(\{\tilde{y}_{z,l,j,n}^{\text{REC}}\}_{n \in \mathcal{N}_l^{\text{REC}} \setminus \{\bar{n}_{z,l,j}\}}; u^{\text{REC}}) f_{z,j}^{\text{REC}}(u^{\text{REC}}) + f_{z,j}^{\text{REC}}(\tilde{y}_{z,l,j,(\bar{n}_{z,l,j})}^{\text{REC}}) \\ &= \bar{y}_{z,l,j}^{\text{REC}} f_{z,j}^{\text{REC}}(u^{\text{REC}}) + f_{z,j}^{\text{REC}}(\bar{y}_{z,l,j,+}^{\text{REC}}), \end{aligned}$$

as $f_{z,j}^{\text{REC}}(0) = 0$ by Assumption 1. Again, a similar result holds for \tilde{y}^{CP} . Therefore, the objectives satisfy

$$\begin{aligned} C_t^{\text{PL}}(\tilde{y}) &= \sum_{z \in \mathcal{Z}} \left(\sum_{j \in \mathcal{J}} \sum_{n \in \mathcal{N}_l^{\text{REC}}} f_{z,j}^{\text{REC}}(\tilde{y}_{z,l,j,n}^{\text{REC}}) + \sum_{k \in \mathcal{K}^{\text{CP}}} \sum_{n \in \mathcal{N}_{l,k}^{\text{CP}}} f_{z,k}^{\text{CP}}(\tilde{y}_{z,l,k,n}^{\text{CP}}) \right) \\ &= \sum_{z \in \mathcal{Z}} \left(\sum_{j \in \mathcal{J}} \bar{y}_{z,l,j}^{\text{REC}} f_{z,j}^{\text{REC}}(u^{\text{REC}}) + f_{z,j}^{\text{REC}}(\bar{y}_{z,l,j,+}^{\text{REC}}) + \sum_{k \in \mathcal{K}^{\text{CP}}} \bar{y}_{z,l,k}^{\text{CP}} f_{z,k}^{\text{CP}}(u^{\text{CP}}) + f_{z,k}^{\text{CP}}(\bar{y}_{z,l,k,+}^{\text{CP}}) \right) \\ &= \bar{C}_t^{\text{PL}}(\bar{y}), \end{aligned}$$

and (\bar{y}, \tilde{x}) has the same objective value in (PMI) as (\tilde{y}, \tilde{x}) has in (P). We have already shown that any feasible solution for (PMI) has a corresponding feasible solution for (P) with the same objective value, so (\bar{y}, \tilde{x}) is optimal for (PMI), as otherwise there must also be a better solution than (\tilde{y}, \tilde{x}) for (P). Therefore, as (\tilde{y}, \tilde{x}) is optimal for (P) and (\bar{y}, \tilde{x}) is optimal for (PMI) with the same objective value, the problems have the same optimal objective. \square

Lemma A.3. *The functions \bar{f}_i defined in (9) have the following properties:*

1. $\bar{f}_i(y) \leq f_i(y)$ for $y \in [y_i^{(1)}, y_i^{(k_i)}]$;
2. \bar{f}_i is concave and continuous; and
3. $\bar{f}_i(y_i^{(j)}) = f_i(y_i^{(j)})$ for all $j \in \{1, \dots, k_i\}$.

Proof. 1. Select j so that $y \in [y_i^{(j)}, y_i^{(j+1)}]$. Then, taking $\lambda = \frac{y - y_i^{(j)}}{y_i^{(j+1)} - y_i^{(j)}} \in [0, 1]$,

$$\begin{aligned} \bar{f}_i(y) &= \frac{y - y_i^{(j)}}{y_i^{(j+1)} - y_i^{(j)}} f_i(y_i^{(j+1)}) + \frac{y_i^{(j+1)} - y}{y_i^{(j+1)} - y_i^{(j)}} f_i(y_i^{(j)}) = \lambda f_i(y_i^{(j+1)}) + (1 - \lambda) f_i(y_i^{(j)}) \\ &\leq f_i(\lambda y_i^{(j+1)} + (1 - \lambda) y_i^{(j)}) = f_i(y), \end{aligned}$$

by the concavity of f_i .

2. Denote $\tilde{f}_i(y) = \min_{j \in \{1, \dots, k_i-1\}} \left\{ \frac{f_i(y_i^{(j+1)}) - f_i(y_i^{(j)})}{y_i^{(j+1)} - y_i^{(j)}} (y - y_i^{(j)}) + f_i(y_i^{(j)}) \right\}$. Consider $y \in [y_i^{(1)}, y_i^{(k_i)}]$ and any index j . If $y \geq y_i^{(j+1)}$, let $\lambda = \frac{y_i^{(j+1)} - y_i^{(j)}}{y - y_i^{(j)}} \in (0, 1]$ so that $y_i^{(j+1)} = \lambda y + (1 - \lambda)y_i^{(j)}$. Then, by concavity of f_i ,

$$f_i(y_i^{(j+1)}) \geq \lambda f_i(y) + (1 - \lambda)f_i(y_i^{(j)}),$$

and

$$\frac{f_i(y_i^{(j+1)}) - f_i(y_i^{(j)})}{y_i^{(j+1)} - y_i^{(j)}} (y - y_i^{(j)}) + f_i(y_i^{(j)}) \geq f_i(y) \geq \bar{f}_i(y).$$

Otherwise, if $y < y_i^{(j)}$, let $\lambda = \frac{y_i^{(j)} - y}{y_i^{(j+1)} - y} \in (0, 1]$ so that $y_i^{(j)} = \lambda y_i^{(j+1)} + (1 - \lambda)y$. By concavity of f_i ,

$$f_i(y_i^{(j)}) \geq \lambda f_i(y_i^{(j+1)}) + (1 - \lambda)f_i(y),$$

and

$$\frac{f_i(y_i^{(j+1)}) - f_i(y_i^{(j)})}{y_i^{(j+1)} - y_i^{(j)}} (y - y_i^{(j)}) + f_i(y_i^{(j)}) \geq f_i(y) \geq \bar{f}_i(y).$$

Finally, if $y \in [y_i^{(j)}, y_i^{(j+1)})$,

$$\frac{f_i(y_i^{(j+1)}) - f_i(y_i^{(j)})}{y_i^{(j+1)} - y_i^{(j)}} (y - y_i^{(j)}) + f_i(y_i^{(j)}) = \bar{f}_i(y).$$

Thus, we have that $\bar{f}_i(y) \leq \tilde{f}_i(y)$. Further, $\bar{f}_i(y) \in \left\{ \frac{f_i(y_i^{(j+1)}) - f_i(y_i^{(j)})}{y_i^{(j+1)} - y_i^{(j)}} (y - y_i^{(j)}) + f_i(y_i^{(j)}) \right\}_{j=1}^{k_i-1}$, so $\bar{f}_i(y) \geq \tilde{f}_i(y)$, and $\bar{f}_i(y) = \tilde{f}_i(y)$. Therefore, as the function \bar{f}_i is a minimum of linear functions, it is continuous and concave.

3. The equality follows from direct evaluation. □

Corollary A.1. Let \bar{f}_i^1 be the piecewise linear function associated with breakpoints $\{y_i^{(j)}\}_{j=1}^{k_i}$ and \bar{f}_i^2 the function with breakpoints $\{y_i^{(j)}\}_{j=1}^{k_i} \setminus \{y_i^{(r)}\}$ for some $r \notin \{1, k_i\}$. Then, $\bar{f}_i^1(y) \geq \bar{f}_i^2(y)$ for $y \in [y_i^{(1)}, y_i^{(k_i)}]$.

Proof. By Lemma A.3, \bar{f}_i^1 is concave. Let j_1 and j_2 be consecutive breakpoints for \bar{f}_i^2 , so

$$j_2 = \begin{cases} j_1 + 1 & j_1 \neq r - 1 \\ j_1 + 2 & \text{otherwise.} \end{cases}$$

Then, by Lemma A.3,

$$\frac{f_i(y_i^{(j_2)}) - f_i(y_i^{(j_1)})}{y_i^{(j_2)} - y_i^{(j_1)}} (y_i - y_i^{(j_1)}) + f_i(y_i^{(j_1)}) = \frac{\bar{f}_i^1(y_i^{(j_2)}) - \bar{f}_i^1(y_i^{(j_1)})}{y_i^{(j_2)} - y_i^{(j_1)}} (y_i - y_i^{(j_1)}) + \bar{f}_i^1(y_i^{(j_1)})$$

for any $y_i \in [y_i^{(1)}, y_i^{(k_i)}]$. Thus, \bar{f}_i^2 can be equivalently constructed in the form (9) by using the concave function \bar{f}_i^1 in place of f_i . It then holds that \bar{f}_i^2 is a piecewise under-approximator of \bar{f}_i^1 and, by Lemma A.3, $\bar{f}_i^1(y) \geq \bar{f}_i^2(y)$ for $y \in [y_i^{(1)}, y_i^{(k_i)}]$. □

Lemma 1. Let $(y^*, x^*) \in \mathcal{X}$ be an optimal solution to (SP). Then, there is an optimal solution that is an extreme point of $\mathcal{X}(y^*)$.

Proof. Denote the optimal cost for (SP) by $z^{\text{SP}} = \sum_{i=1}^n \bar{f}_i(y_i^*) + \sum_{\omega \in \Omega_1} p_\omega c_\omega^T x_\omega^*$. Consider the restricted problem

$$z^{\text{RP}} = \min_{(y,x) \in \mathcal{X}(y^*)} \sum_{i=1}^n \bar{f}_i(y_i) + \sum_{\omega \in \Omega_1} p_\omega c_\omega^T x_\omega. \quad (\text{RSP})$$

As $\mathcal{X}(y^*) \subseteq \mathcal{X}$, (RSP) is a restriction of (SP), and $z^{\text{SP}} \leq z^{\text{RP}}$. However, (y^*, x^*) is feasible for (RSP), so $z^{\text{RP}} \leq z^{\text{SP}}$. Thus, the optimal values $z^{\text{RP}} = z^{\text{SP}}$, and an optimal solution for (RSP) is also optimal for (SP).

Further,

$$\mathcal{X}(y^*) = \{(y, \{x_\omega\}_{\omega \in \Omega_1}) \geq 0 : y_i = y_i^* \ \forall i \in \llbracket n_I \rrbracket, Ay = b, B_\omega x_\omega + Dy = d_\omega \ \forall \omega \in \Omega_1\}$$

is a polytope under the assumption that \mathcal{X} is bounded. Lemma A.3 gives that the functions \bar{f}_i are concave, so the objective function of (RSP) is concave and (RSP) is a concave minimization over a polytope. Thus, (RSP) has an optimal solution at an extreme point of $\mathcal{X}(y^*)$ by Lemma A.1. This solution is also optimal for (SP), and therefore, there is an extreme point of $\mathcal{X}(y^*)$ that is optimal for (SP). \square

Theorem 3. *Algorithm 1 terminates finitely with a global optimum of (SCP).*

Proof. Consider the set of feasible realizations of the integer components of y ,

$$\mathcal{Y} = \{z \in \mathbb{Z}_+^{n_I} : \exists (y, x) \in \mathcal{X}, y_i = z_i \ \forall i \in \llbracket n_I \rrbracket\} \subseteq \{z \in \mathbb{Z}_+^{n_I} : \underline{y}_i \leq z_i \leq \bar{y}_i \ \forall i \in \llbracket n_I \rrbracket\}.$$

Clearly, \mathcal{Y} is finite. We construct the set of points that are extreme points of $\mathcal{X}(z)$ for some $z \in \mathcal{Y}$,

$$\mathcal{E} = \bigcup_{z \in \mathcal{Y}} \{(y, x) : (y, x) \text{ extreme point of } \mathcal{X}(z)\}.$$

This set is also finite, as there are finitely many extreme points of any polytope $\mathcal{X}(z)$ and finitely many such $z \in \mathcal{Y}$. We next construct the set of unique capacity solutions with a corresponding extreme point:

$$\bar{\mathcal{E}} = \bigcup_{(y,x) \in \mathcal{E}} \{y\}.$$

Then, $|\bar{\mathcal{E}}| \leq |\mathcal{E}|$, so $\bar{\mathcal{E}}$ is finite.

For any y feasible for (SP) or (SCP) and any set of breakpoints $\{y_i^{(j)}\}_{j=1}^{k_i}$ generated by Algorithm 1,

$$y_i^{(1)} = \underline{y}_i \leq y_i \leq \bar{y}_i = y_i^{(k_i)}$$

by the initialization in step 1 of the algorithm, so $y_i \in [y_i^{(1)}, y_i^{(k_i)}]$. As a result, the first property of Lemma A.3 will apply for any feasible solution y to these problems. Further, $y_i^{(1)}$ and $y_i^{(k_i)}$ maintain the same values across iterations by step 5 of the algorithm.

Suppose that Algorithm 1 produces a sequence of iterates $(\tilde{y}^s, \{\tilde{x}_\omega^s\}_{\omega \in \Omega_1})$ of length at least $|\bar{\mathcal{E}}| + 1$. We note that (SP) has a finite optimal solution by the boundedness assumption on \mathcal{X} (Lemma A.1). Under Assumption 2, at every iteration s , the iterate $(\tilde{y}^s, \{\tilde{x}_\omega^s\}_{\omega \in \Omega_1})$ is an extreme point of $\mathcal{X}(\tilde{y}^s)$, so $\tilde{y}^s \in \bar{\mathcal{E}}$ for all s .

As the number of iterates is strictly larger than $|\bar{\mathcal{E}}|$, some capacity solution must be revisited, so $\tilde{y}^{s_1} = \tilde{y}^{s_2}$ for some $s_1 < s_2 \leq |\bar{\mathcal{E}}| + 1$. Denote the set of breakpoints at the start of iteration s_2 by $\{y_i^{(j)}\}_{j=1}^{k_i}$. Note that the breakpoints which generate $\bar{f}_i^{s_1}$ are a subset of those which generate $\bar{f}_i^{s_2}$ and include $\{y_i^{(1)}, y_i^{(k_i)}\}$, so

$\bar{f}_i^{s_2}(\tilde{y}_i^{s_1}) \geq \bar{f}_i^{s_1}(\tilde{y}_i^{s_1})$ as a consequence of Corollary A.1. From step 5 of the algorithm, either $\tilde{y}_i^{s_1} \in \{y_i^{(j)}\}_{j=1}^{k_i}$ or $\bar{f}_i^{s_1}(\tilde{y}_i^{s_1}) \geq f_i(\tilde{y}_i^{s_1})$ for each i . In the former case, $\bar{f}_i^{s_2}(\tilde{y}_i^{s_2}) = f_i(\tilde{y}_i^{s_2})$ by Lemma A.3. In the latter case,

$$\bar{f}_i^{s_2}(\tilde{y}_i^{s_2}) = \bar{f}_i^{s_2}(\tilde{y}_i^{s_1}) \geq \bar{f}_i^{s_1}(\tilde{y}_i^{s_1}) \geq f_i(\tilde{y}_i^{s_1}) = f_i(\tilde{y}_i^{s_2}).$$

Thus, the condition in step 4 of the algorithm is met at iteration s_2 , and Algorithm 1 terminates finitely within $|\bar{\mathcal{E}}| + 1$ iterations.

Let the algorithm terminate at iteration s with iterate $(\tilde{y}^s, \{\tilde{x}_\omega^s\}_{\omega \in \Omega_1})$. Then,

$$\begin{aligned} \sum_{i=1}^n \bar{f}_i^s(\tilde{y}_i^s) + \sum_{\omega \in \Omega_1} p_\omega c_\omega^T \tilde{x}_\omega^s &= \min_{(y, \{x_\omega\}_{\omega \in \Omega_1}) \in \mathcal{X}} \sum_{i=1}^n \bar{f}_i^s(y_i) + \sum_{\omega \in \Omega_1} p_\omega c_\omega^T x_\omega \\ &\leq \min_{(y, \{x_\omega\}_{\omega \in \Omega_1}) \in \mathcal{X}} \sum_{i=1}^n f_i(y_i) + \sum_{\omega \in \Omega_1} p_\omega c_\omega^T x_\omega \\ &\leq \sum_{i=1}^n f_i(\tilde{y}_i^s) + \sum_{\omega \in \Omega_1} p_\omega c_\omega^T \tilde{x}_\omega^s \\ &\leq \sum_{i=1}^n \bar{f}_i^s(\tilde{y}_i^s) + \sum_{\omega \in \Omega_1} p_\omega c_\omega^T \tilde{x}_\omega^s, \end{aligned}$$

where the first inequality follows from Lemma A.3 and the third from the termination criterion in step 4 of the algorithm. Therefore,

$$\min_{(y, \{x_\omega\}_{\omega \in \Omega_1}) \in \mathcal{X}} \sum_{i=1}^n f_i(y_i) + \sum_{\omega \in \Omega_1} p_\omega c_\omega^T x_\omega = \sum_{i=1}^n f_i(\tilde{y}_i^s) + \sum_{\omega \in \Omega_1} p_\omega c_\omega^T \tilde{x}_\omega^s,$$

and $(\tilde{y}^s, \{\tilde{x}_\omega^s\}_{\omega \in \Omega_1})$ is a global optimum for (SCP). \square

References

- Dai Q, Spangenberg J, Ahmed S, Gaines L, Kelly JC, Wang M (2019) EverBatt: a closed-loop battery recycling cost and environmental impacts model. Technical report, Argonne National Lab.
- Horst R, Pardalos PM, Van Thoai N (2000) *Introduction to Global Optimization* (Springer Science & Business Media).
- Xu C, Dai Q, Gaines L, Hu M, Tukker A, Steubing B (2020) Future material demand for automotive lithium-based batteries. *Communications Materials* 1:99.